Topological Optimization of the CubeSat Frame Using the Finite Element Method

by

Vajiheh _(Hasti) AsgharzadHamidi

Submitted in partial fulfilment of the requirements for the
degree of Master of Applied Science

At

Dalhousie University

Halifax, Nova Scotia

September 2020

I dedicate this to my parents Zarintaj and Saied and my brother Ali, and all my family, particularly my husband, Alireza, and my son, Radin, for their support without them my engineering education would have been impossible.

TABLE OF CONTENT

LIST OF TABLES

LIST OF FIGURES

ABSTRACT

The material selection, design, manufacturing method, and in-service environmental conditions, such as temperature and vibration, are all critical factors in the design of a CubeSat nano-satellite. Furthermore, as weight is a critical factor, to make a lighter CubeSat for space research, it is considered to use aluminum alloys. If considering the use of flexible additive manufacturing, various aluminum alloys may be suitable, while some are not. As an example, AlSi10Mg could be a suitable alloy to construct a CubeSat, as it has been successfully used in additive manufacturing.

In the first part of the thesis, the Nano-Racks CubeSat Deployer (NRCSD) system is illustrated, in terms of the requirements for small satellite launches. This system will be explained in the part (2-3-2) of the thesis. The defined requirements exerted on all parts of the mission will be examined.

In the second part of the thesis, the concept of topological optimization (TO) during design, along with additive manufacturing technology are explained, and then the aluminum alloys which can be produced by additive manufacturing method are investigated. In the third Chapter, the designed CubeSat, which resulted from applying the TO method, subjected to different loading in a simulated launch/space environment is investigated. Optimization of the designed CubeSat in this part is done using the NISA software. The results due to applying loads and adequate boundary conditions (BC) helped to design an optimized CubeSat in TO. Final design and approving of the CubeSat design in launch circumstances can be assessed by doing FEA on the shape in NISA. In the fourth Chapter, the validity of the CubeSat design, by introducing some major tests, has been investigated. In the fifth Chapter simulation results of two different kinds of CubeSats are shown, to validate the methods of FEA application.

LIST OF ABBREVIATIONS USED

CDH	Command and Data Handling
CCP	Canadian CubeSat Project
EVR	Extravehicular Robotics
FOD	Foreign Object Debris
I/F	Interface
ISS	International Space Station
ITU	International Telecommunication Union
JAXA	Japan Aerospace Exploration Agency
NASA	National Aeronautics and Space Administration
NRCSD	Nano-Racks CubeSat Deployer
PD	Payload Developer
PDU	Power Distribution Unit
TO	Topological Optimization
US	United States

ACKNOWLEDGEMENTS

I wish to dedicate my deepest gratitude to Prof. Kevin Plucknett for his financial support and professional advice, and also thank Prof. Farid Taheri for his patience and encouragement to enable me to finish this thesis. I want to express my gratefulness to my parents Zarintaj and Saied, my husband Alireza, and my brother Ali for their moral support. I cannot imagine having been able to finish my studies, without their unreserved love and encouragement.

Finally, my sincere gratitude goes to all the people who shared part of their life experience with me that helped to have, hopefully, a more realistic mentality.

CHAPTER 1 INTRODUCTION

A mathematical method that gives a design with an optimized material (mass) is called topological optimization (TO) or shape optimization. The finite element method (FEM) can be used for TO formulation and evaluating the design presentation. Researchers in aerospace, mechanical and civil engineering have been widely working on TO applications, while engineers can subsequently further contribute to this by adding constraints to the formulation for developing the manufacturing purposes.

The application of additive manufacturing (AM) technologies are evolving and further developing in a variety of current industries at a rapid pace. AM of aluminum alloys has received attention from industrialists and researchers due to its high potential for lowering mass, strengthening of components, and the ability to manufacture three-dimensional (3D) components that are not feasible through other methods. However, the number of Al alloys that are presently usable in laser-based 3D printers is quite limited. Despite that, one of the aims of continuing AM studies is to increase the range of suitable alloys and the variety of AM techniques that are devised, in order to remedy these issues.

In recent years, the fast-growing small satellite industry has been developing internationally, and the manufacturing of nanosatellites known as ‘CubeSats’ has been increasing rapidly. CubeSats are based on 10 x 10 x 10 cm “modules” that can be added in a single linear dimension, up to a nominal maximum size of 60 x 10 x 10 cm. Compared with the traditional large satellites, for space exploration missions in recent decades, increasing numbers of CubeSats have been applied due to a variety of advantages, such as low cost and relatively short development cycles. CubeSats can be used in isolation or multiple units, in what is known as a ‘constellation’ of nanosatellites.

The present study focuses on the use of FEM to assess the effects of different acceleration and thermal conditions on a variety of 1U CubeSat designs, generated through TO by finite element analysis.

1.1 Introduction

A first attempt towards the development of a nanosatellite standard is the CubeSat program. A cube-shaped nanosatellite design of a 10 cm side length is called CubeSat. CubeSats are miniature satellite units, with a basic building block of 10 x 10 x 10 cm (for a 1U satellite), and a weight of up to ~1.3 kg. By convention, nanosatellites are defined as being between 1 and 10 kg in mass, while picosatellites are between 0.1 and 1 kg in mass, and hence both terms can be applied to CubeSats, depending upon their operational mass. A CubeSat works alone or in a 'constellation' group of multiple units that can interact with each other. There are four main types of operational purposes for CubeSats: technology demonstration, science, educational learning and commercial mission [1]. The first three of these are covered within the Canadian CubeSat Project (CCP) remit. The CCP program, initiated in 2017 by the Canadian Space Agency, is focused on the development of CubeSats within Canadian university environments. The internal structure of a CubeSat needs to contain a broad range of functional systems, including an antenna and radio communication system, power source (i.e. Li-ion batteries), and computer(s) that control all the functions of the satellite. Installing the antenna on the exterior is also possible, which is also the location for the photovoltaic solar panels that are required for energy generation, as the CubeSat must be self-sustaining in operation. The CubeSat will also likely carry a 'payload' of some form, for example, environment sensors, cameras, etc. The primary goal of the present

work is to optimize the design and modelling approaches for CubeSat chassis, which would ultimately be fabricated using (for example) aerospace-grade Al-based alloys when subjected to the mechanical stresses and vibrations arising during rocket launches and ultimate deployment.

Mass, stiffness and strength requirements are the most significant factors in the design of structural space systems [2]. To a large extent, the survivability of the instrumentation depends on the stiffness; also, by reducing the weight of the chassis structure while retaining mechanical performance, an increase in the payload is potentially possible, which may help to decrease the launch costs. Choosing the proper material is essential, due to a large percentage of the CubeSat mass being within the structural and mechanical parts of the satellite [3].

Up to now, more than 1200 CubeSat missions have been successfully launched into space. Descriptions relating to a wide range of CubeSats missions, and their capabilities, can be found in the literature [4]. Access of small payloads into the environment of space is the primary mission of the CubeSat program [5]. The initial choice for the material(s) used in the chassis structure is Al-based alloys, with the most common grades being AA6061 or AA7075, respectively, because of having low densities, moderately low thermal expansion coefficients, combined with relatively high strength and stiffness.

CubeSat must have compatibility with the nanosatellite deployer, and a number of systems are available, such as the Poly-Picosatellite Orbital Deployer (P-POD), developed by California Polytechnic (or CalPoly), or the Nano-Racks CubeSat Deployer (NRCSD), which will be used for the CCP. This compatibility is necessary to ensure the safety and success of the mission. CubeSat ejection into orbit, known as deployment, is possible by

sliding the satellite along a series of rails (Figure 1.1). The rectangular aluminum box with a spring mechanism door is often called the P-POD [5], based on the original CalPoly design.

Figure 1.1 Inside of the P-POD [5].

Aluminum alloys are one of the best choices for CubeSat applications, or any satellite for that matter, due to their low weight, combined with high strength and stiffness. Some of the other comparable stiffness-to-weight materials are Mg, Ti and CFRP. Specifically, one of the main aims of the current study is to investigate such Al alloys in terms of their design to produce complex-shaped, topologically optimized and crack-free components, ultimately using laser-based AM approaches. An effort is also made to select/determine the material properties in a relatively rapid, low-cost manner. The chosen options for optimizing performance will be validated by comparing a series of computational simulations through the use of the FEM. The mechanical and thermal loading will also be taken into account during the evaluation. It should be noted that vibration during the launch of such satellites to the International Space Station (ISS), where they are subsequently deployed, will be significant.

1.2 Problem Statement and Motivation

One of the essential areas of scientific exploration is in space, and it used to be largely performed through the launch of traditional satellites. However, in the past few decades, miniaturization of small space exploration devices has been developed [6]. Mass, stiffness, and strength requirements are significant specifications that need to be met for the design of structural space systems. For the survivability of the instrumentation, a specific level of stiffness is required. By reducing the weight, one can increase the payload, which decreases the effective launch cost (as the mission capacity is increased) and thus can extend the mission objectives. A large percentage of the CubeSat's mass is represented by the satellite's structural and mechanical parts of the chassis, and it shows the importance of choosing appropriate material(s) to minimize the weight. Nowadays, researchers can complete some limit space explorations at relatively low costs and, in the academic area, this field has resulted in the development of picosatellites (<1kg) and nanosatellites (<10kg), which have been developed for many years focusing attention on reducing the size and mass in terms of incorporating advanced technologies [2]. By comparing to traditional satellites that have considerable size and mass, the advantages of CubeSats represented by smaller size, lower costs, and rapid fabrication [2] are clear. So, FEM for topological optimization (TO) optimizes the material design of the CubeSat under the defined loads and boundary conditions within a specified space. Chapter 3 shows the results of TO and FEA in NISA software. In principle, therefore, the application of 3D printing technologies is an approach with relatively short development cycle advantages. However, the costs of laser-based 3D printing are still high. So for the continuing rapid

development of pico- and nanosatellites, the combination of CubeSat concepts and 3D printing technology is favourable [6].

1.3 Thesis Objectives

Despite the vast body of works relating to the performance in terms of the topic of finite element design of CubeSats, to the best of our knowledge, no investigations have been made in terms of the shape optimization (i.e. TO) of the CubeSat to address the Al alloy material, AlSi10Mg, in particular by using laser-based AM methods. The research undertaken in this dissertation plans essentially to assess this issue, with the objective of applying shape optimization, using TO, and improving the material use/chassis design through addressing the required design criteria of high strength, lightweight, and low cost. In brief, the overall objective of the study is to optimize the shape of the CubeSat chassis design and develop a relatively inexpensive and robust CubeSat concept for typical engineering applications in the space sector where relatively light CubeSats are required, as with the other aerospace-related applications. As noted earlier, such an approach of minimizing the chassis mass allows an increase in the payload weight or allows the fabrication of a satellite with an overall lower mass.

1.4 Thesis Organization

This thesis has divided into six chapters. The first chapter provides a basic introduction and thesis structure. Chapter 2 contains a literature review which deals with the subject of CubeSats in more detail. The discussion begins with a review of CubeSat types and the associated Nano-Racks deployer system, with a focus on finite element analysis and shape

optimization. Moreover, additive manufacturing technologies as a method for manufacturing CubeSats are also discussed in this chapter. Chapter 3 discusses the finite element analysis and TO approaches used for the CubeSat design by applying NISA TO software, and the influence of acceleration, thermal loading, and vibration on the final shape of the CubeSat. In Chapter 4, for investigation and validation of the study, a series of tests such as functional, vibrational and thermal testing is introduced. Chapter 5 discusses the simulation analysis (FEA) of two studies with the current study. Chapter 6 provides the overall conclusions and recommendations for future work.

CHAPTER 2 LITERATURE REVIEW

2.1 Introduction

In 1999 the first idea of designing a small cubic shaped satellite, known as a CubeSat, was initiated by Bob Twigg and Jordi Puig-Suari [7]. Since the inception of the concept, in 2000, nearly 1,000 CubeSats have been launched into earth orbit [7]. The primary purpose of designing CubeSats was for educational purposes, specifically for helping students become acquainted with the space science engineering environment. However, CubeSats are now used for a variety of scientific, governmental, and commercial purposes. Students working on these kinds of engineering projects can design and build CubeSats at a relatively low cost and are provided with an interdisciplinary labour experience. It is expected that the number of launched CubeSats will continue to grow, as it has increased in the last eight years. Although CubeSats are a high demand satellite unit, the failure and destruction of the CubeSat system are high, too [8]. Figure 2.1 shows the number of launched CubeSats in the last eight years, which has increased dramatically.

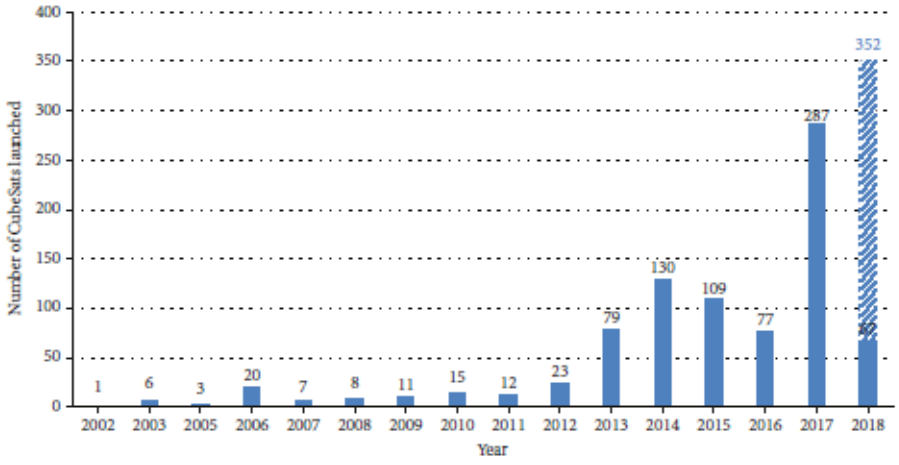

Figure 2.1 Number of launched CubeSats between 2005-2018 [9].

One of the most critical outcomes in designing the small CubeSat is exploring space in low-Earth orbit (LEO). Usually, one-unit (1U) CubeSats are used for university projects to develop CubeSat plans for the first time [10]. Figure 2.2 shows a small one-unit satellite.

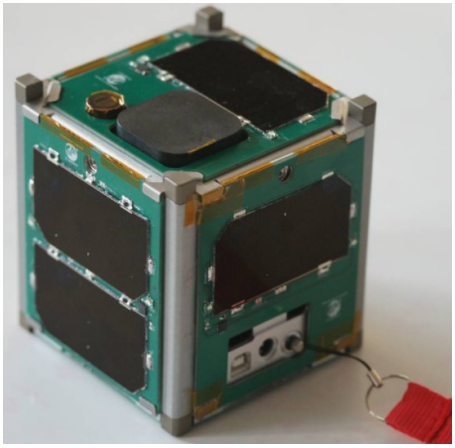

Figure 2.2 A small satellite with one unit CubeSat [10].

2.2 The Canadian CubeSat Project

The Canadian CubeSat Project (CCP) is a prominent project, funded through the Canadian Space Agency (CSA), that will ultimately culminate in a real space mission, with satellites deployed from the ISS (https://www.asc-csa.gc.ca/eng/satellites/cubesat/default.asp). In April 2017, the CCP introduced the idea of allocating university professors to involve their students in the space project. In this project, the successful teams have been offered a unique opportunity of CSA funding for manufacturing their CubeSat.

Experts of the CSA are responsible for guiding professors and students to optimize each mission successfully. The CCP will consequently provide experience in a variety of areas of space science and technology, including communicating the work to the public and preparing students to become the innovators of Canada's next generation of space scientists

and engineers [1]. The design of the Dalhousie CubeSat, funded through the CCP, started in March 2018, and it will continue until the end of 2021. The construction and testing are expected to happen between August 2020 to December 2021 ('flatsat' testing is already underway as of July 2020), with an expectation to launch to the ISS in the Spring or Summer of 2022.

2.3 CubeSats

The various international CubeSat programs have developed in some universities, private companies, and government organizations due to the low-cost of developing the CubeSat satellites [11]. CubeSats have become an exciting innovation in the world of space research and applications, with objectives for a variety of space aspects such as education, science, and defence, being pursued. Initially, researchers were using CubeSats only in low Earth orbit (LEO) for communications, but recently they have even been planned for deployment around the moon, Mars moons and potentially even Jupiter moons and Saturn moons [12]. In our solar system, there are more than 200 moons with different shapes and sizes, some of them have atmospheres and oceans. The cold, dusty, desert world with a thin atmosphere is the fourth planet in the solar system with the name of Mars. Jupiter is the giant planet in the solar system, and Saturn is the second largest one [13]. Up until May 31st, 2018, the total number launched CubeSats was 855. Currently, the leading application sector for CubeSats, remote sensing, corresponds to about 45% of all launches. Now, with the development of CubeSats, a total of fifty-eight countries have already been involved [9]. While CubeSats are small satellites, with weights significantly less than 300kg (1100 lb), they must still be approved to a specific series of standards for controlling the factors such

as shape, dimensions and mass [14]. As noted earlier, the first launches of CubeSats were in the early 2000s, and they were very simple satellite designs to achieve the demands of student education or to meet some amateur needs.

A CubeSat can operate solely or in a group of multiple units (maximum 24 units) as a 'constellation'. Figure 2.3 shows the different units of CubeSats, which can work in four types of missions: technology demonstration, science, educational and commercial missions.

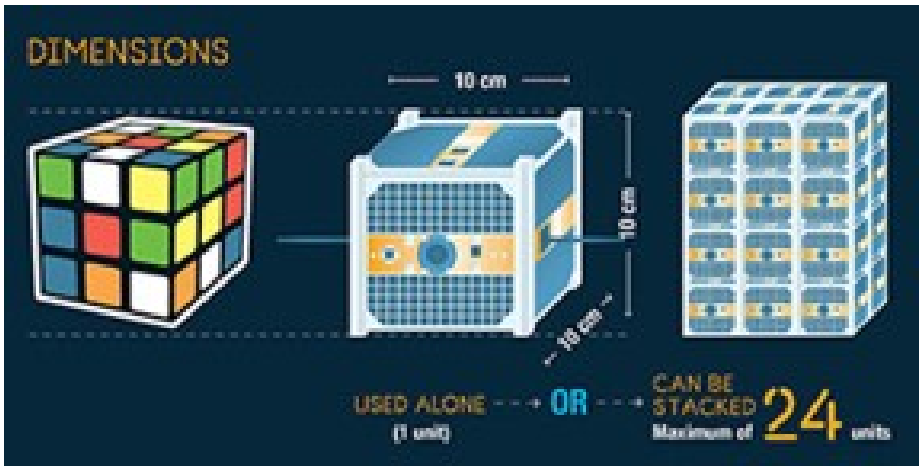

Figure 2.3 Different types of CubeSat [1].

The expected length of a cube-shaped (1U) pico-/nanosatellite is 100 mm per side, and it may not weigh more than ~1.3 kg for every single 1U CubeSat. So, for double (2U) and triple (3U) designs, they should weigh be less than ~2.6 kg and ~3.9 kg, respectively. The dimension for a double is 227 mm, and 340.5 mm for a triple; the changes should apply on the Z direction only, so the X and Y dimensions are fixed (at 100 mm) [5].

In the launch scenario, the CubeSat must be strong enough to survive launch without damage or dimensional change in the deployer. The cube's edges need to have a minimum radius of 1 mm, to ensure smooth movement within the confines

of the deployer. The two crucial structural requirements of the rails are to have flat faces and rounded corners (around 1 mm radius) [5].

Figure 2.4 shows an example of a 1U CubeSat. It contains a frame, different panels, power board, command and data handling (CDH), electronics, payload electronics, a camera, and the actual payload. CDH is the system for controlling the other CubeSats subsystems such as communication, ACDS (attitude determination and control subsystem) and payload[15].

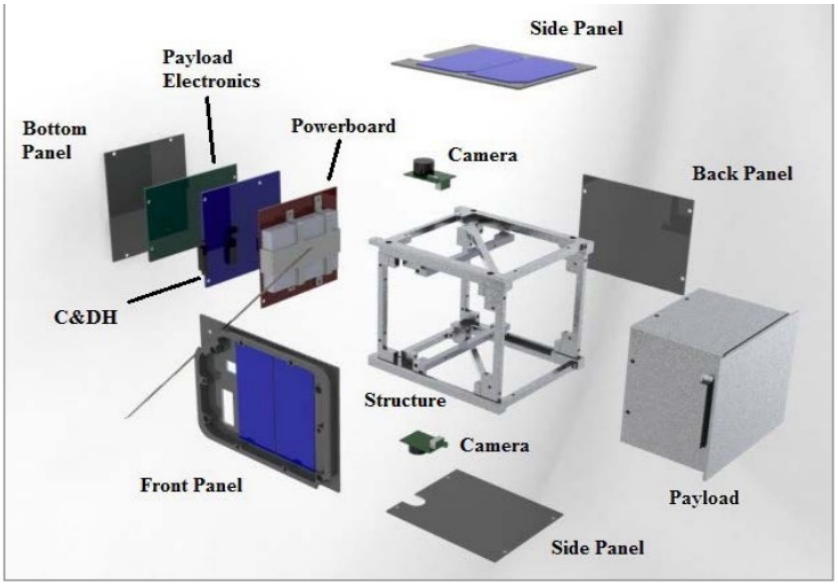

Figure 2.4 Example of 1U CubeSat [5].

CubeSats need to have some general requirements to allow a regular mission operation. Firstly, they are entirely self-contained from the moment they are charged in the deployer and then transported to the ISS. Any supports or charging of batteries is prepared after ending the integration. Secondly, during the launch, detachable parts, or the creation of any

space foreign object debris (FOD) is forbidden. Thirdly, the fragile materials used for solar cells should meet suitable approval requirements [16]. In terms of the electrical system requirements, during the launch, any electronics must not be active due to avoiding any electrical interference (or interface (I/F)) with the launch vehicle. CubeSats have rechargeable batteries, and during the launch, they must be fully deactivated. Below there are some operational requirements for integration and the related legal obligations for the safety of the CubeSats and associated systems (e.g., the ISS):

1- The capability of receiving the transmitter shutdown command for CubeSats with rechargeable batteries.
2- The antenna and solar panels may be deployed a minimum of 30 seconds after ejection of the CubeSat from the deployer.
3- Preparing an orbital FOD reduction plan by developers and obtaining the approval documentation with NASA space debris mitigation rule recorded in NASA Technical Standard (NASA-STD-8719.144).[5].

2.3.1 Inside of The CubeSat

A bus module in a CubeSat is made of anodized aluminum and saves a whole board containing avionics. A microwave radiometer in the payload performs the primary science mission and receipt millimetre-wave radiometer pictures of storms, and the whole module spins, which helps the radiometer be calibrated from the cosmic space during the rotation. The other advantage of spinning is allowing the sensor to observe the full zone [17]. Based on the CubeSat Standard Kit (CSK), a MicoMAS-1 avionic stack is designed by Pumpkin Inc, and it involves a series of boards and standard pin mappings. The attitude determination and control system (ADCS), I/F board, and the avionics I/F board are

examples of the custom boards used to create the electronics systems to ensure success for the mission.

The scanner assembly is located just beneath the payload module and allows the spinning of the payload. The top I/F board is located on the left side (Figure 2.5) of the scanner assembly; it involves the motor controller and some other parts.

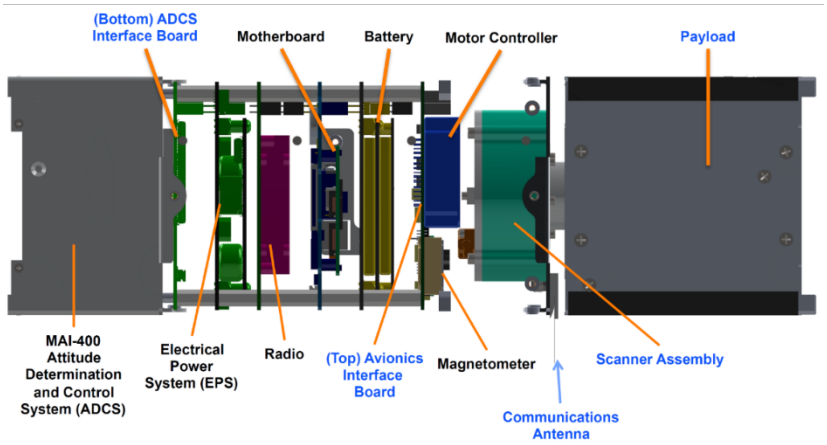

Figure 2.5 Bus design of a MicroMAS-1 [16].

Below the battery, the motherboard is located with an on-board computer (OBC) and the radio communication board.

The top I/F board is installed beneath the scanner assembly. The motor controller and some other power distribution units (PDUs) are in the top I/F board (Figure 2.6).

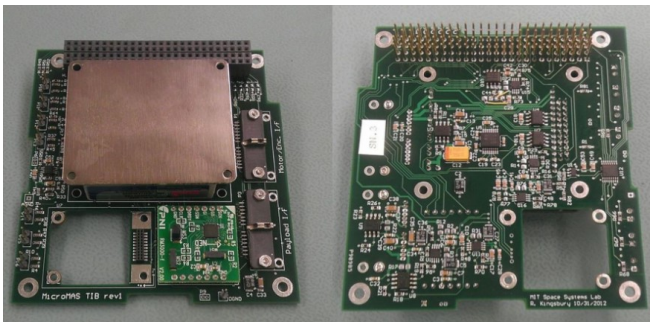

Figure 2.6 Top I/F board [16].

Below the motherboard, the radio communication board is located. It carries a nanosatellite radio, and a custom carrier card was made to transfer the data to the right pins on the bus. PDUs in the top I/F board and the radio communication board controls power to the radio and stores data for the time that CubeSat is not connected with NASA's flight facility (Figure 2.7).

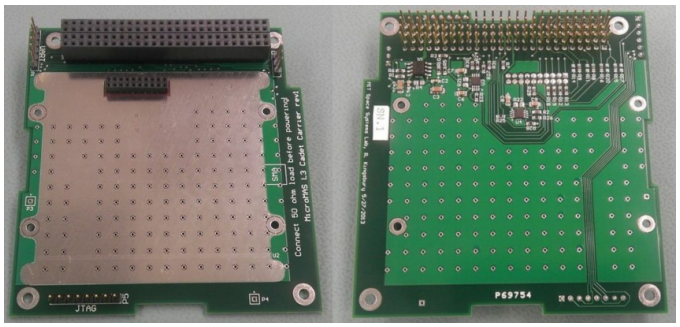

Figure 2.7 Top of the radio carrier board (left) and bottom of the radio carrier [16].

Below the communications board, the electrical power system (EPS) is located. Its duty is managing the onboard power and gathering electricity produced by the solar panels, and then it charges the batteries and distributes energy to the systems that need it (Figure 2.8).

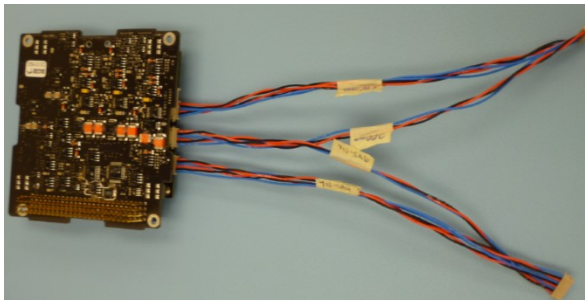

Figure 2.8 Electrical power system [16].

After the ADCS, the bottom I/F board is located, and it is attached with a board to board I/F connector. There is a PDU on the baseboard, and it supplies power to ADCS. In addition, an I/F allows transferring data to the ADCS from the sun sensors, which are on the surface of the CubeSat (Figure 2.9) and allow a determination of the satellite orientation.

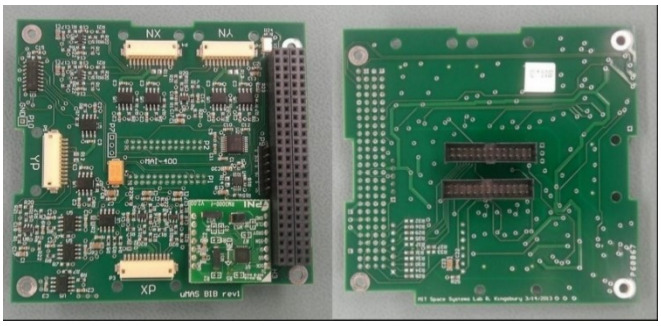

Figure 2.9 Bottom I/F board [16].

At the base of the CubeSat, the ADCS is located, and its duty is helping the orbit stability and orientation, and reducing momentum produced by the spinning payload. A variety of sensors and actuators help achieve this (Figure 2.10) [16].

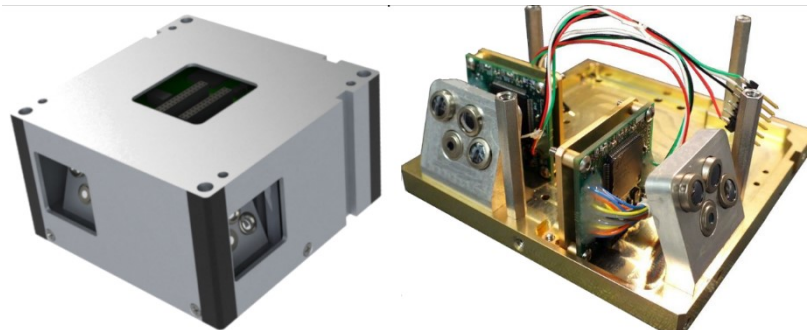

Figure 2.10 ADCS (left) and static earth sensor (right) [16].

2.3.2 Nano-Racks CubeSat Deployer System (NRCSD)

The Nano-Racks CubeSat Deployer System (NRCSD) is a rectangular tube made of anodized aluminum plates, a base plate assembly, and deployer doors. Both the NRCSD and Poly-Picosat Orbital Deployer (P-POD) systems are used to deploy the CubeSats into space, and both designs can hold up to six 1U CubeSats, or combinations of 1U, 2U, 3U, 4U, and 5U CubeSats up to a six-unit maximum. Alternatively, the deployers can hold a single 6U (unit) satellite. CubeSats must have compatibility with either the NRCSD or P-POD requirements, such as the dimensions, maximum mass, and the launch/operational restrictions. The inside walls of the NRCSD are smooth, to minimize friction and hence

minimize the possibility of jamming of the CubeSat within the deployer. Between the interior walls and deployable CubeSat systems, there should not be any intentional contact [16]. The potential for jamming is a serious consideration, as if the first unit to be deployed jams, all the remaining CubeSats would be trapped within the deployer and could not be launched.

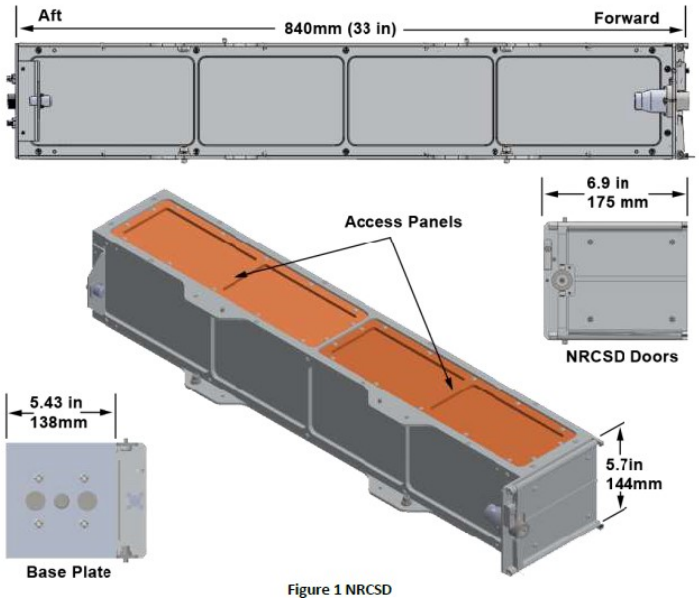

Figure 2.11 Nano-Racks CubeSat Deployer system (NRCSD) [15].

The accessibility of CubeSats once in the deployer tube is located only on the top face of NRCSD, with suitable access panels, as shown in Figure 2.11. In Table 2-1, the mass of NRCSD is given according to the maximum ballistic number (BN), which is allowable for ISS deployed payloads [16].

Table 2-1 Mass properties of CubeSat.

Unit	Maximum Mass (kg)
1U	2.82
2U	5.657
3U	8.485
4U	11.314
5U	14.142
6U	16.971

2.3.3 Testing Requirements

For the safety of the CubeSats and the deployer, some testing requirements need to be done before launching. These tests must meet all launch providers (e.g., Nano-Racks, NASA, etc.) requirements. The following tests show the minimum ones that must be met for all CubeSats.

1- Testing random vibrations at a higher level (more than launch vehicle).

2- Having proper outgassing of components in a thermal vacuum bakeout.

3- Filling an acceptance checklist for visual inspection and measurement of the critical regions of the CubeSat Figure 2.12). Additional testing, according to the integrated system of the CubeSats, will be represented [5].

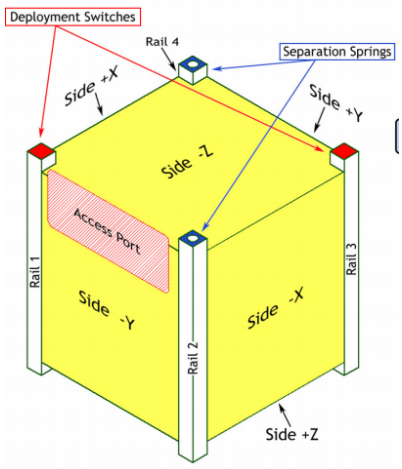

Figure 2.12 Isometric drawing of CubeSat [5].

2.3.4 Environmental Requirements

2.3.4.1 Acceleration Loads

The below table shows the acceleration loads in all six directions, so the structures should be designed to survive in the accelerations documented, and potentially for scenarios when all of them are acting simultaneously.

Table 2-2 Launch load factors.

	Nx (g)	Ny (g)	Nz (g)
Launch	+/- 7.0	+/- 4.0	+/- 4.0

All of the safety-critical structures must be identified to determine the requirements for verification. The safety-critical aspects are considered in all CubeSats designs, because of the need to avoid failure of the elements and the associated production of space debris; they could potentially impact with ISS visiting vehicles (which is known as a catastrophic hazard in terms of ISS strategy) [18].

2.3.4.2 Vibration

The random vibration comes from one of the most intensive loads for the satellite's integrity, which occurs during the launch [2]. In addition, the capability for withstanding random vibration conditions should be considered for a flight in terms of the relevant safety requirements. For designing the structure, different features like strength, material and shape are studied. Aluminum alloys are the materials of the underlying chassis construction in the system. Al-based alloys are lightweight (Al has a density of ~2.6 g/cm^3) and have high resistance under the loading conditions. In some design software packages, the complete satellite construction can be modelled. For instance, by using commercial FE software, NISA, ANSY, ABAQUS and LS-DYNA, the assembled model meshes can be

utilized for analyzing the design. Under the given loading situation(s), static, modal, and harmonic analysis are studied to assess the integrity of the CubeSat shape during loading. These analyses are undertaken to make sure the satellite system will survive during launch loads and be deployable once into space. The investigation is clarified by neglecting all extra holes in the form due to having a minimal shape. The following equation shows the simple equation for evaluating of the first natural frequency of a beam with one end fixed:

$$f_1 = \frac{1.875^2}{2\pi}\sqrt{\frac{EI}{mL^4}} \quad (1)$$

where the area moment of inertia is I, the length of the beam is L, E is the modulus of elasticity, and the mass of the beam is m. The three analyses are performed as outlined below:

1- The Static Analysis is for estimating the stress, strain, displacements, and forces in the structure. The weight of the satellite system and the gravitational force of (g-force), in this analysis, are applied to the center of the entire satellite with the fixed bases on the bottom [19].

2- In Modal Analysis, the fundamental frequency of the whole structure must be ≥30 Hz, according to global stiffness requirements. This frequency will help the entire system to survive during the launch. In this modal analysis, to obtain the frequencies and mode shapes of structure, the dynamic loading condition is needed [17].

3- Harmonic analysis, like the static one, is conducted to obtain the maximum stress on the system.

The structure of the satellite is designed to stand its centre of mass within (1-2) cm spatial resolution. For strengthening the entire structure, a simple model is introduced, and the analysis is done under the given loads (Table 2-2). For instance, the maximum stress and deformation in a 2U CubeSat are obtained as 3.415 MPa and 1.63 x 10^{-4} m, respectively, which shows the max-stress is less than the yield strength of the material (i.e., aluminum alloy AA 7075). The results are shown in Figure 2.13. So, both of these values are within the control limits [19].

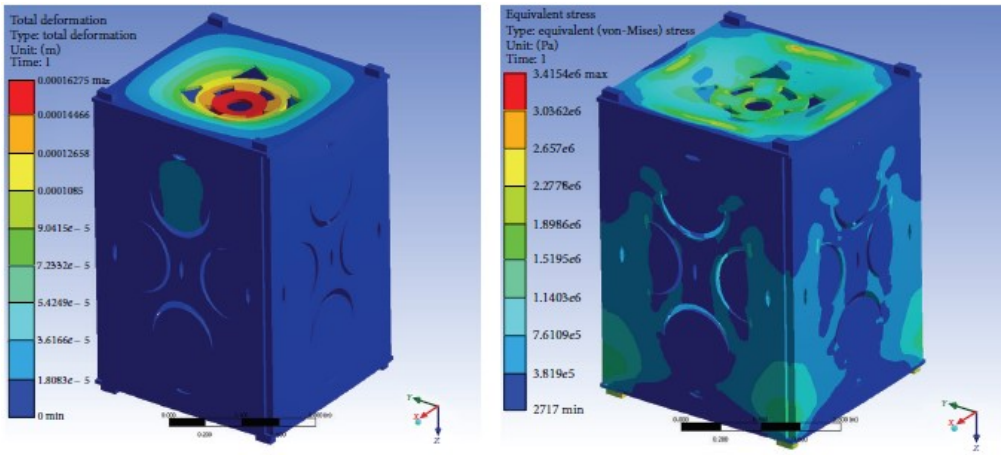

Figure 2.13 Deformation (Left) and stress (Right) [19].

2.3.4.3 Thermal Condition

A proper design that also accounts for the thermal loads would guarantee a successful mission in the harsh environment [20]. In different missions there are different expected thermal environments which are shown in Table 2-3 and the solar loading conditions which are dictated by JAXA, -60 degrees and 73 degrees of beta angle condition, should be taken into account [18].

Table 2-3 Expected thermal conditions.

Phase of Mission	Expected Temperature
Ground Transport	Different for each payload
Ground Processing (Nano-Racks))	Different for each payload
Ground Processing (NASA/JAXA)	10 °C to 35 °C
Dragon pressurized (Cargo)	18.3 °C to 29.4 °C
Cygnus Pressurized Cargo)	10 °C to 46 °C
HTV Pressurized (Cargo)	0 °C to 50 °C
On-orbit, Pre-deployment	16.7°C to 28.3 °C
On-orbit, EVR Pre-deployment	-10 °C to 45 °C

2.4 The Technology of Additive Manufacturing

Additive manufacturing (AM), also known as 3D printing or rapid prototyping, is utilized in a variety of manufacturing environments to create a complex structure, relatively rapidly. AM allows the construction of components that simply cannot be manufactured using conventional technologies. AM describes the technologies which manufacture 3D objects by the addition of material 'layer by layer'. Initially, computer-aided design (CAD) software was used for drawing the final shape, including all details, and then converting the CAD design to a .stl file (standard tessellation language). These files typically break the component up into individual layers that, when combined, produce the final component. These layers are then what is actually printed by the AM method chosen [21]. AM technology was created more than 20 years ago and is starting to be widely used in numerous applications, such as aerospace, biomedical, automotive, and other areas. In addition, this method of manufacturing has been employed to create small size prototype segments for analysis and experimental checks in terms of the related material [22].

This technology is a revolution in the product manufacturing industry, and it is changing the way of designing the products and organizing new businesses. The greatest benefit of AM methods is the ability to produce components, often in one piece (hence avoiding joins)

that simply are impossible to produce otherwise. AM relies on preparing the drawing using 3D CAD and designing the model by computer, which means that design modifications can be relatively simply implemented in the CAD figures. AM technology is also a method for the reduction in production steps, regardless of the complexity of the part being built. So even for complex shapes, by AM technology, the component can essentially be built in a single step. AM technology can, therefore, help to eliminate the number of processes and parts within a component. For instance, the traditional component may need a variety of moulds and fixtures, or careful planning for CNC machining, which can be messy and time-consuming [21]. However, it is important to note that some post-AM processing is still often required, such as heat-treatment(s) or final machining.

2.4.1 Selective Laser Melting Method (SLM) or Laser Powder Bed Fusion (LPBF)

Selective Laser Melting (SLM) is one of the prominent techniques which is used in the AM industry with powder bed processes [23]. One AM method that utilizes a powder bed (e.g., Polymer, Metal or even Ceramic) to produce a part from a 3D CAD file is known as a selective laser melting (SLM) or laser powder bed fusion (LPBF) [24]. Parameters like poor powder flowability, high humidity and low laser power impact the quality of the final part. Four parameters that are affecting the imparted energy density function Ψ according to equation [25]:

$$\Psi = \frac{p}{v.h.d} \tag{2}$$

where p is the power of the laser *(W),* the scan speed is v , the scan spacing is h, and the width of the covering of powder deposited is d. Thus, by increasing the power of the laser,

it is clear that the laser energy imparted into the material increases as well. Although equation (2) is relatively simplified, it should really be modified to add laser diameter, and its angle with the surface of the melt, the gas flow direction and so on. For producing aluminum alloy parts, the SLM process has been studied in recent decades. The aluminum alloys with prominent potential for future AM work can be considered due to having a low density. During the SLM building process, the mechanical behaviour of parts differs from the traditional fabrication methods, due to the rapid heating and cooling speeds. As a consequence, it can be hard to control the final properties for aluminum alloy parts produced by this method. A variety of defects can arise, such as porosity, cracks, low quality of surface and property anisotropy. The principal industrial aluminum alloys are those that are most often attempted to be implemented in SLM technology.

A list of the principal aluminum alloys that have been evaluated for SLM is listed in Table 2-4. It is interesting to note that the AlSi10Mg alloy produced by SLM is an example of a material with higher mechanical properties than the equivalent one provided by casting. Having components prepared with high strength aluminum alloys has significant potential for using these alloys for the automotive, defence and aerospace industries [24]. Fabrication of Al-based composites by the SLM/LPBF method is also attractive due to the possibility of reducing the weight by combining complex geometries and netting structures [26], such that the material volume used is reduced while maintaining suitable properties.

2.4.2 Thin Wall Structures in AlSi10Mg Alloy

Some natural durable and lightweight structures such as bone, sponge, etc. have also led to the creation of analogous porous materials necessary for biological applications. Producing thin-wall structures are possible with the LPBF method by using suitable processing

strategies. A computer-controlled fibre laser in LPBF can melt the layer of metal powder and produce complex 3D parts. Manufacturing thin wall products in an AlSi10Mg alloy build can result in a low weight, high thermal conductivity, high strength, and corrosion-resistant structure for the aerospace and automotive industries [27].

Table 2-4 The studied aluminum alloys in SLM [24].

Family	Alloys	Feasibility by SLM	
		Susceptibility to cracking	Part density
		+ : not	+ : $d_{rel} \geq$
		Susceptible	99%
		0 :	0 :
		susceptible	97 % $< d_{rel}$
			$< 99\%$
		- : very	- : $d_{rel} \leq 97$
		susceptible	%
		n.s : not said	n.s : not said
1XXX	Al	+	n.s
2XXX	AlCu2	-	n.s
	AlCu5	0	n.s
	AlCu6.8	+	n.s
	AlCu11.8	+	n.s
	AlCu5Mg (2022)	-	+
	AlCu4Mg1 (2024)	0	+
	AlCu6Mn (2219)	0	+
	AlCuMg	0	+
	AlCu2Mg1.5Ni	+	n.s
	(2618)		
4XXX	AlSi7Mg0.3 (A356)	+	+
	AlSi7Mg0.3 (A357)	+	
	ALsI20Fe5Cu3Mg1	+	
	AlSi20	+	
	AlSi12	+	
	AlSi50	+	
	AlSi10Mg	+	
	AlSi12Mg	+	
	AlSiNi	+	
5XXX	AlMg5.7	+	
	AlMg6	+	
	AlMgScZr (Scalmalloy)	+	
6XXX	AlMg1SiCu (6061)	0	-
7XXX	AlZn5	0	n.s
	AlZn2	0	n.s
	AlZn10	0	n.s
	AlZnMgCu	n.s	n.s
	AlZn5.5MgCu (7075)	-	0
8XXX	AlFe8.5V1.35Si1.7	+	+
	(FVS0812 ou AA8009)		
NC	Al($(Fe_2O_3)5$	n.s	n.s
	AlNdNiCo	+	+

2.4.2.1 Materials and Procedure

A fibre laser system, such as Yb (Ytterbium), is capable of melting powders with a non-stop power up to 200 W, and with a 100 μm spot and up to 7000 mm/s scanning rate in an argon environment. A substrate temperature of 100 °C for the production platform would be suitable to decrease the residual thermal stress between the fused material and the substrate. In addition, for controlling the laser movement to define the laser scanning path remotely and with high accuracy, a galvanometer electro-optical device can be used. Figure 2.14 shows an example of an AlSi10Mg powder used for SLM/LPBF, where the diameters are 10% (d_{10}), 50% (d_{50}) and 90% (d_{90}) full size distribution of 12.87 μm, 27.06 μm and 42.59 μm, respectively.

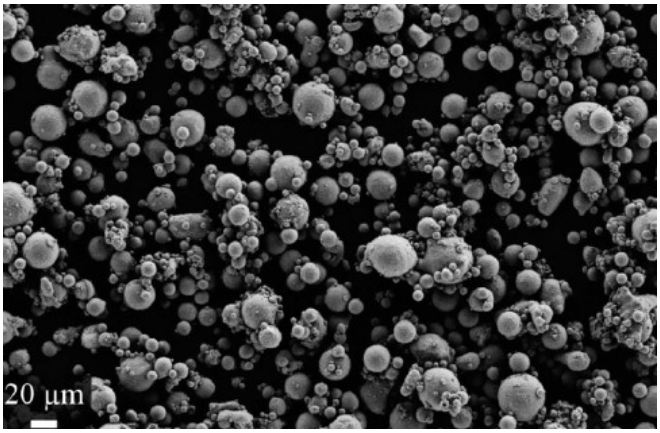

Figure 2.14 AlSi10Mg powders [27].

2.4.2.2 Design Considerations

For designing lightweight components for automotive, aerospace, and biomedical demands, the features can have 1 mm or less thickness, which is near the limit of the SLM/LPBF procedure. In terms of the laser's operating parameters and scanning method in this process, the size of the melt pool, while melting the metal powder within the laser scan track, can be defined by the minimum size of the feature, and it affects the geometrical

and mechanical specifications. The importance of this will increase when other unpredictable aspects like energy changes, powder quality and morphology, are examined. Some defects such as internal voids, un-melted powder inclusions and unusual shapes, created by the LPBF process, can be observed. Figure 2.15 shows a schematic diagram to describe the parameters of the process. The parallel laser tracks or identical laser passes with equivalent laser radiation, melt the powder material by moving a tiny dimension laser beam across the surface. Hatch spacing distance, which is the distance between consecutive laser passes, is usually constant in the entire process, and it is identified by laser point scale, constant scan speed and laser-powder interplay [28].

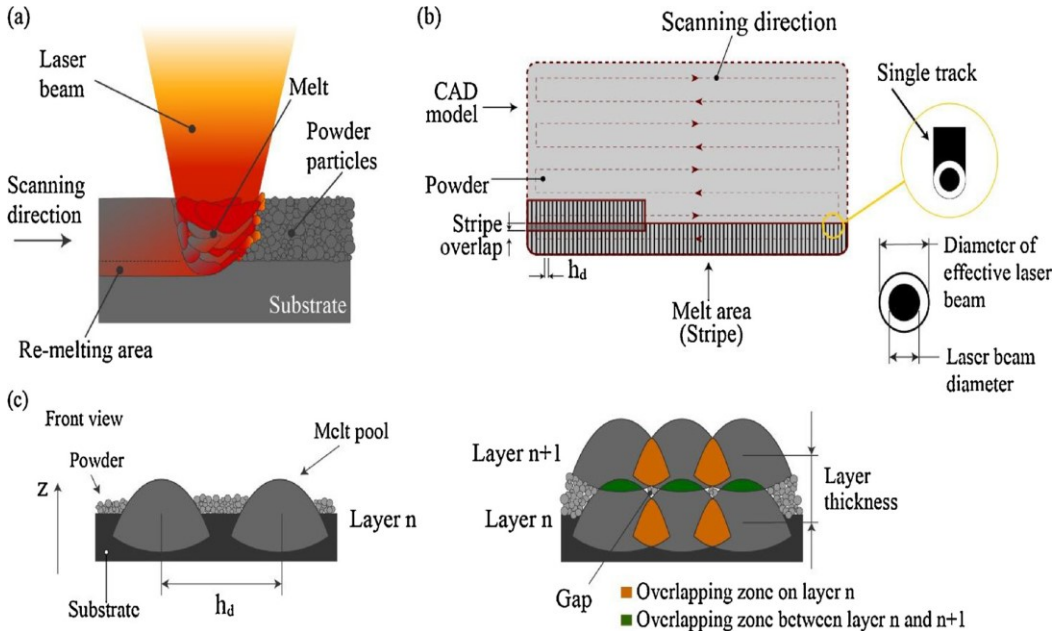

Figure 2.15 (a) Schematic for laser melting method; (b) Showing policy from the top view; (c) Front view of overlapping the scan tracks and different layers [28].

Physical characteristics in the materials and the energy density can define the developed melt pool [28]. Below, equation (10) shows the energy density, which is a calculation for an average of the applied energy (by volume of material) through the scanning of a layer:

$$E = P/(v.h_d.t) \; or \; E = 4P/(\pi.d^2.v) \quad (3)$$

where P is the laser power, v is scanning speed, t is the layer thickness, and the hatching distance is h_d. In terms of the dimension, shape and solidification response of the melt, energy density effects the durability of the melt pool. Because of heat conductivity, the temperature in the edge of the melt pool is lower than in the middle region. The shape of the track and its continuity are impacted by this effect. The overlapping happens due to the layer-by-layer production method, and a re-melting process occurs between the top and bottom layers [27]. The quality of manufacturing can be changed even with the same energy input. For instance: according to equation (3), combining the low power and slow speed of scanning or on the contrary, high power and high speed of scanning, the quality changes. In addition, the scanning speed influences the hatching distance (Figure 2.15 c). Too small of hatching distance makes a too large melt line, due to an excess of overlapping, and with too big of a hatching distance there is not any overlapping. The deposition would then appear as if created by discontinuous dots and the porosity could emerge within the segments. Overlap and re-melting will be happening because of the layer by layer fabrication strategy.

2.4.3 Observation of SLM/LPBF Manufacture of AlSi10Mg

A series of prior experiments for analyzing the manufacture of thin wall structures in AlSi10Mg by LPBF were conducted and thin wall structures built in the x and y directions have been investigated [27] [29]. Therefore, the effect of the fabrication methods for manufacturing AlSi10Mg alloys with thin walls through the use of LPBF technology, and some of these results, are summarised below:

1- Fabrication of a dense, thin wall of AlSi10Mg is possible, in terms of having adequate process parameters available for the LPBF procedure to be successful.

2- The energy density, as a metric for comparing the parts manufactured with the LPBF method (in terms of a variety of deposition restrictions), was not able to gather data about the complexity of the melt pool in this study.

3- The behaviour of the alloy is different in terms of building the aluminum with parallel walls (along x-direction) or perpendicular walls (along y-direction), due to the orientation with respect to the movement of the recoating blade. Fabrication along the x-direction, with high laser power, rapid scan rate and 0.4 mm hatching distance, led to the formation of regular walls and continuous shape; in contrast, the y-direction led to wall deformity. The irregularities might be due to failures in the wall structure[27] along the y-direction, because of the friction forces which are created by contact between the walls being built and the re-coater paddles.

4- It was shown to be feasible to evaluate the wall's real width by a regression model, and these kinds of thin walls can be fabricated with regular laser power, scan speed, and hatching distance values.

5- The experimental equations for an objective build model in AlSi10Mg alloy are used to define the data, which is obtained by a comparison between the as-designed and as-fabricated thin walls. Consequently, the model can explain how to decrease the in conformity that happens to the as-designed morphology and geometry of the thin-walled parts manufactured by LBPF [27].

2.4.4 Advantages of Using Additive Manufacturing Method

The way of designing and manufacturing is changing through use of the additive manufacturing (AM) method. This fabrication method, when compared with the traditional ones, offers the possibilities of application in space sector with the below advantages [30] [31] :

1- In short time scales, the possibility of fabricating lots of component sections.
2- One step fabrication.
3- Decreasing the number of parts and limitation of the number of joints.
4- Possibility of reducing weight with new designs achieving certified structural properties.
5- With a decrease of fabrication time and material used, environmental impact and power consumption in fabrication decrease as well.
6- Optimization in process speed.
7- Possibility to fabricate complex shaped components.
8- Capability of creating composites with double extruder for fiber and matrix. This permits making a specific design for embedding bolts or reinforcing defined parts of the component.
9- Embedding wiring or sensors in multiscriptual structures is possible.
10- Enforceability to a variety of materials: metals, composites, or ceramics.
11- Some evidence for the feasibility of in-orbit or on-planet fabrication.

CHAPTER 3 TOPOLOGICAL OPTIMIZATION (TO) AND FEA IN NISA

3.1 Topological Optimization (TO)

The first satellite design optimization, improvement, analysis and testing verification was performed by the University of Patras Satellite (UPSat) [2]. The purpose of the innovation involves manufacturing the structure by using aluminum instead of composite components. Mass, stiffness, and strength are the prominent requirements in the design of space structures. High stiffness helps to ensure the survivability of the instrumentation and lowered weight increases the payload and consequently reduces the effective launch costs. In product design, the shape has a unique impression. The shape is determined by technical requirements, construction, materialization method, and fabricating technologies [32]. A mathematical method that optimizes material layout by using FEM within the design space is called TO. Various solutions in the past years for specific problems in engineering have been proposed. There are two classical and advanced techniques for optimization. The classical methods, for finding the optimum solution of differentiable functions, can be used. These methods are limited in practical applications and sometimes lead to a set of nonlinear equations simultaneously, which are difficult to solve. The numerical methods are the advanced techniques of optimization which used in software [32]. For this specific study, NISA software has been selected. NISA software incorporates one of several optimization techniques that can be employed to find the optimum shape and size of engineering parts under different restraints like stress, displacement, buckling inconsistency, kinematic consistency, and natural frequency. For conducting TO using FEM, initially, we need to create a simple and preliminary design for the component shape with the exact boundary

dimensions, and then mesh it with an adequate mesh type. A proper mesh helps to find the area(s) for material elimination and preparation of a new component layout within the initial boundaries. The proper mesh in NISA for doing TO is a tetrahedral mesh. The important aspects of tetrahedral mesh production and optimization are the local changes, which means removing edges or faces. Therefore, other elements of the mesh will not change after local improvement in mesh quality [33]. In the optimization process, after creating a proper mesh and applying boundary conditions (BC), the output of the used software will terminate with several results in different files. The number of shapes depends on the complexity of the initial component shape and the applied loads it will operate under, and the last step would be the final design generated from TO.

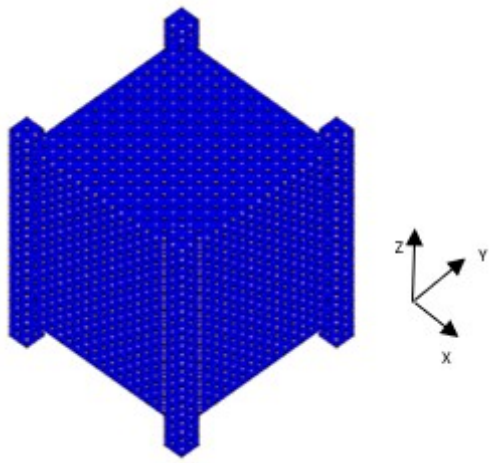

Figure 3.1 The initial shape of IU CubeSat with tetrahedron mesh.

Figure 3.1 shows the initial approximate design of a 1U CubeSat prepared using the NISA software. It is an empty (10 x 10 x 10 cm) cube with 5mm thickness. It is suggested to apply accelerations separately, and step by step. By applying accelerations in all directions simultaneously, the results are not satisfactory for designing of the final shape, since the regions to be eliminated could not be exactly defined. The first results are illustrating after

applying the acceleration on the whole body in the x-direction only. The last even four steps of this optimization are shown in Figure 3.2.

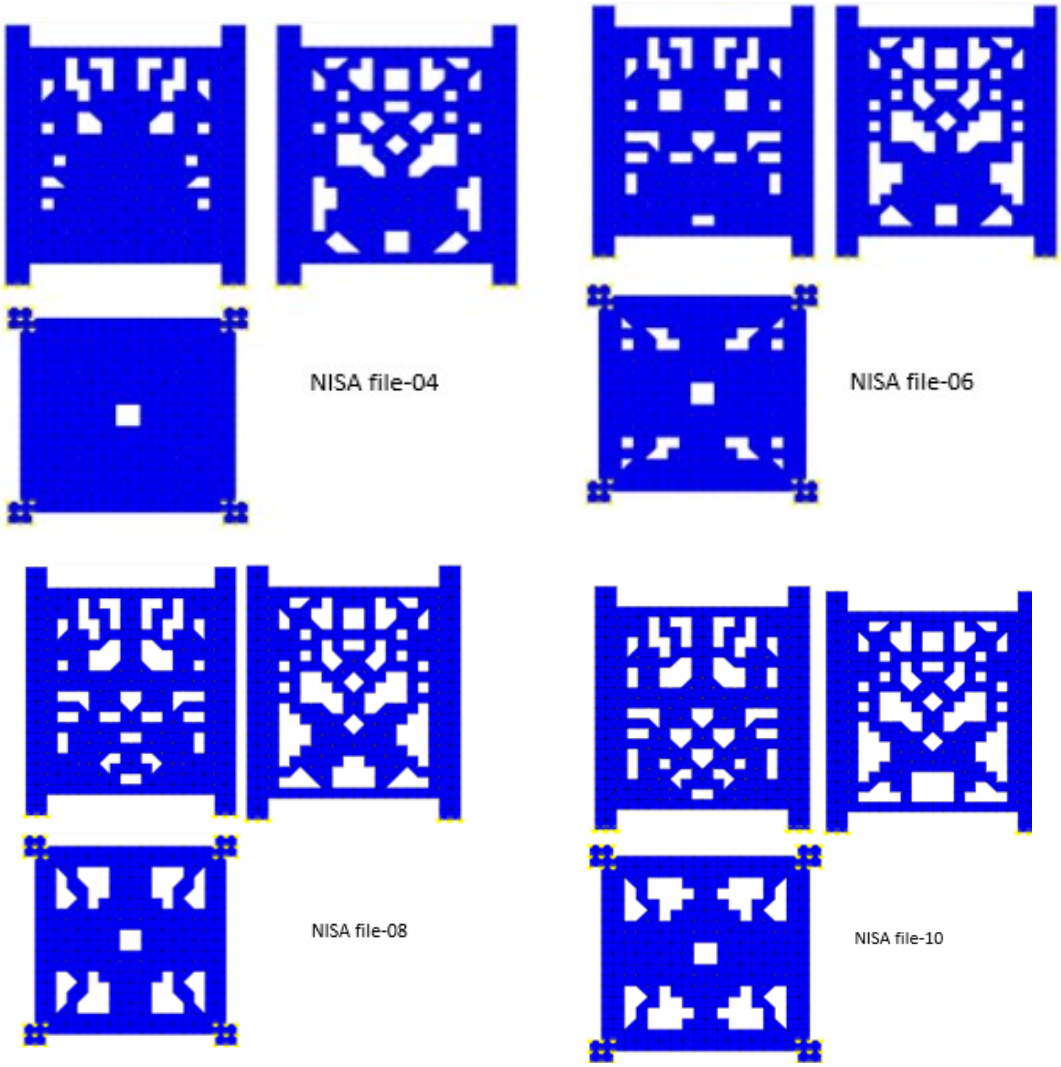

Figure 3.2 Four steps of TO results under the X-acceleration in NISA.

In step file-04, the top view has only created a hole in the center of the cube, but in the last NISA file (file-10) in Figure 3.3 shows that more elements has been eliminated. Figure 3.3 demonstrates the TO results under acceleration in the y-direction.

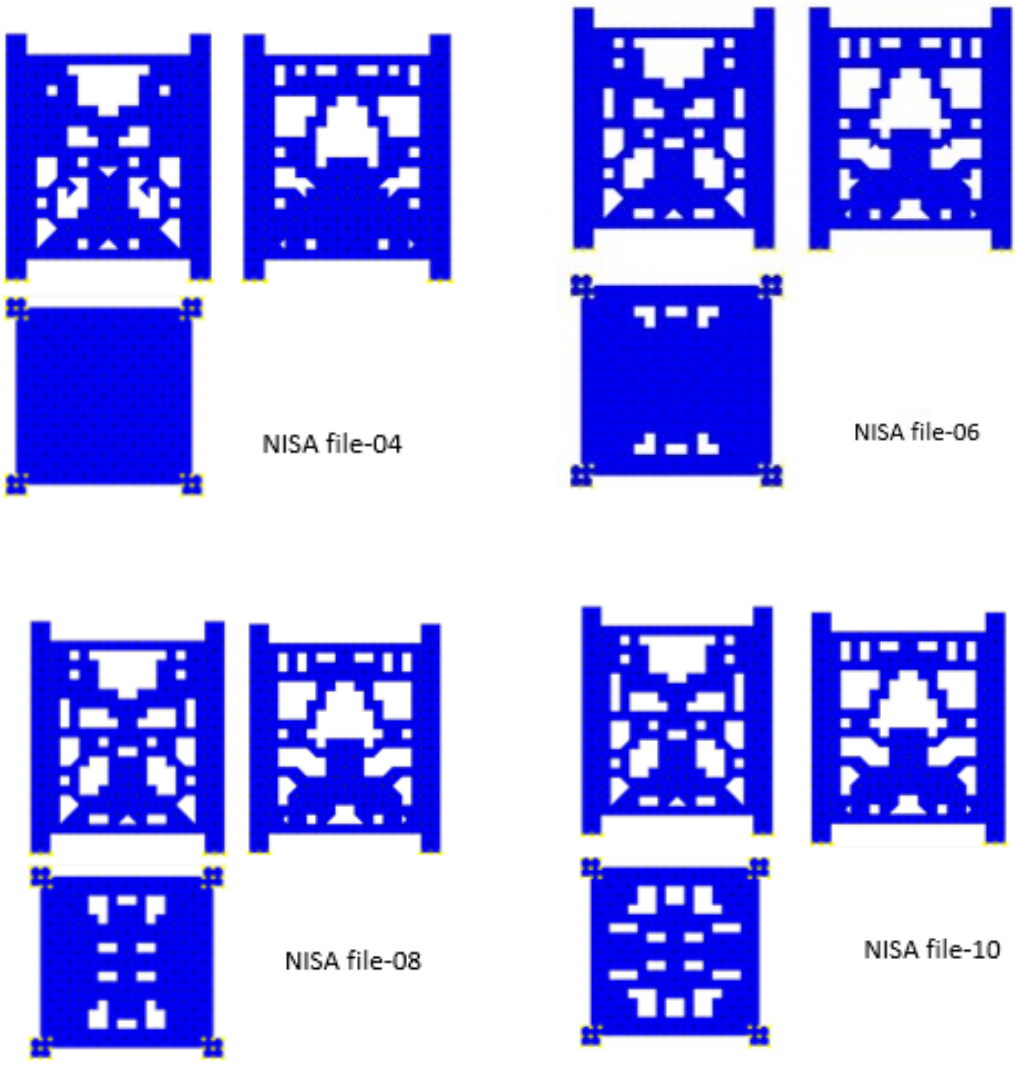

Figure 3.3 Four steps of TO results under the Y-acceleration in NISA.

Due to having a tetrahedral mesh, the eliminated regions do not have smooth edges, and this needs to be a build consideration for designing the ultimate shape.

In the last step, the results in Figure 3.4 demonstrate TO under the z-acceleration direction.

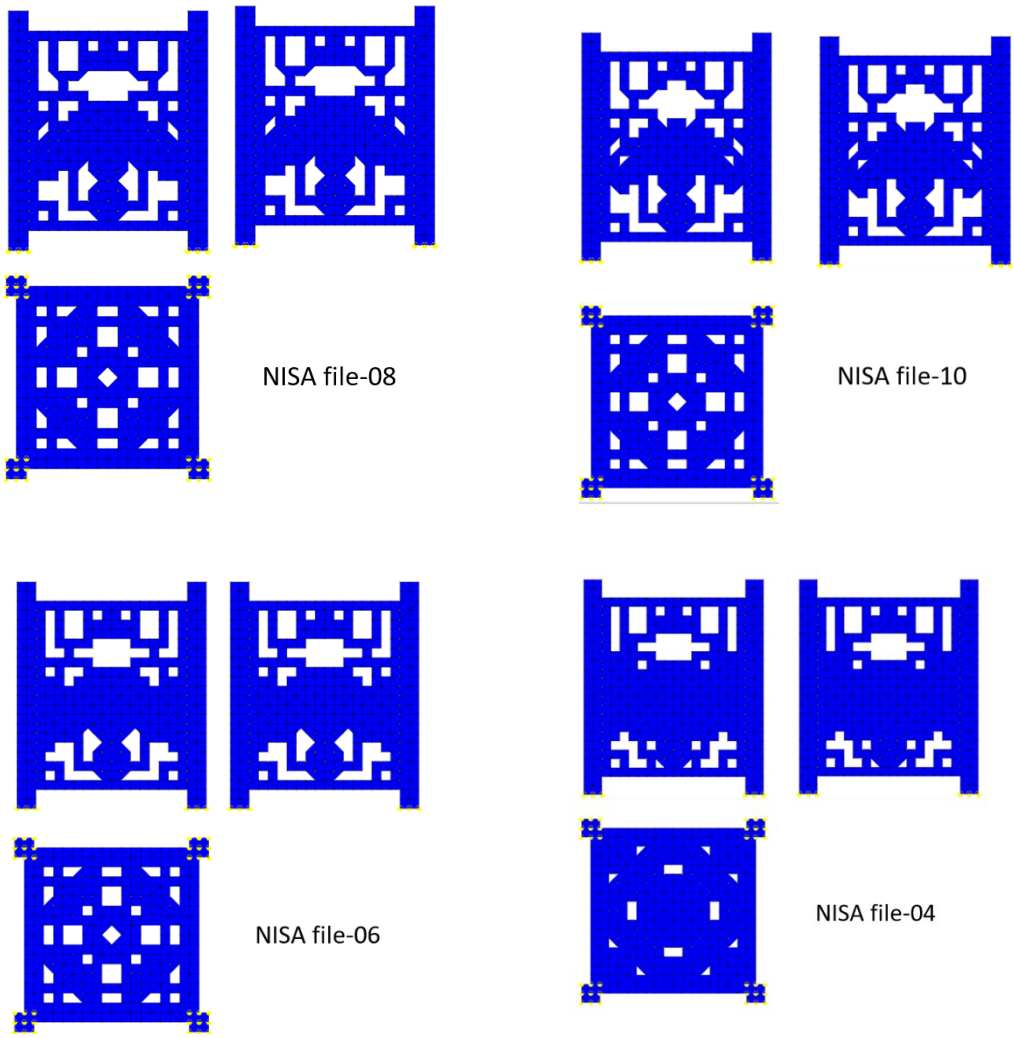

Figure 3.4 Four steps of TO results under the Z-acceleration in NISA.

Subsequently, the accelerations can be combined in all three x, y and z directions. By combining all of the results in all directions, the optimal shape can be created. Figure 3.5 is one of the optimized results in terms of combination x-acceleration, y-acceleration and, z-acceleration. The exact size of holes and curves in the sharp edges, created by TO in NISA, have been designed step by step to avoid having any concentrated stress in those areas.

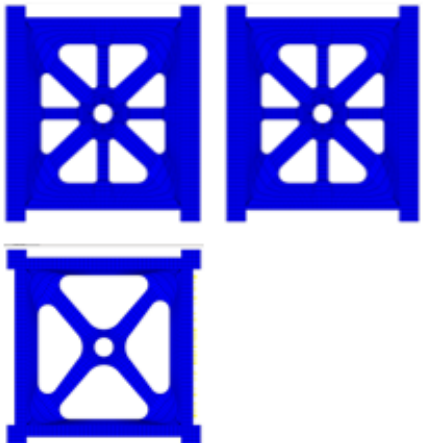

Figure 3.5 The final optimized shape of the cube.

The next part (part 3.2) of the analysis is using FEA on this final optimized shape to confirm that the design is adequate under the defined load and acceleration circumstances.

3.2 Revisiting the Configuration

Above analyses have been set the primary structural shape through a TO analysis. But in the second stage it needs to obtain a new practical assembly configuration for installing the inside parts of CubeSat. Additive manufacturing method helps to reduce the number of parts in order to establish improvements in assembly configuration phases and it is one of the main goals in this study. This easier integration is known as an innovative assembly configuration [31].

There are two types of analysis:

1- Creating innovative structural shapes as the primary design resulted by TO analysis.

2- Designing an assembly configuration. This design of the CubeSat must contain main parameters such as CubeSat rails with the standard shape and dimensions, maximum overall mass, defined by standard, is 1.3kg,

The idea of designing the traditional CubeSat by AM production can potentially bring a new assembly concept, which means a remarkable reduction of parts in satellite structure. Figure 3.6 Shows a possible structure with two parts.

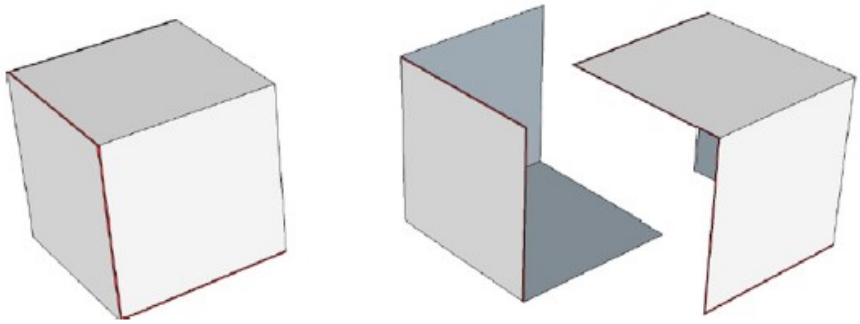

Figure 3.6 Assembly logic [31].

Figure 3.7 shows another alternative assembly option for designing a 1U CubeSat.

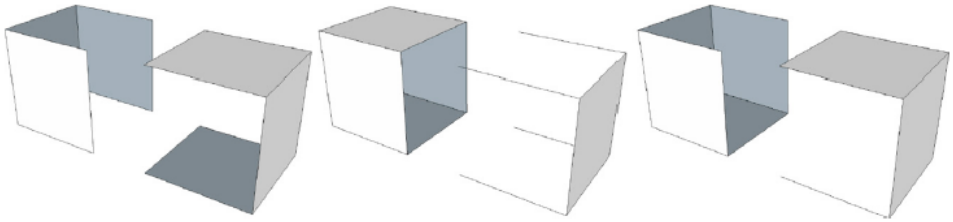

Figure 3.7 Alternative assembly options [31].

After following such an assembly strategy, the proper method of the assembling the CubeSat parts and interlocking system is the first proposed design. Figure 3.8 shows an interlocking system which uses simple dove tail locking. not,

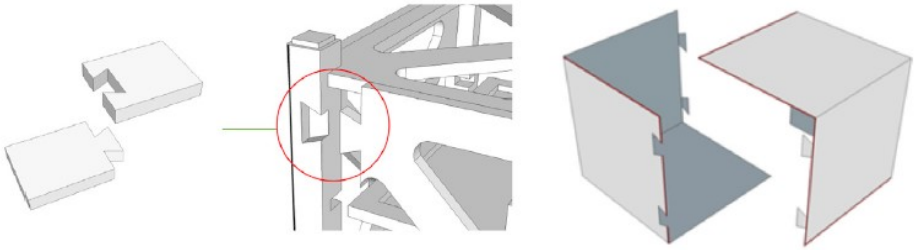

Figure 3.8 Interlocking model description [31].

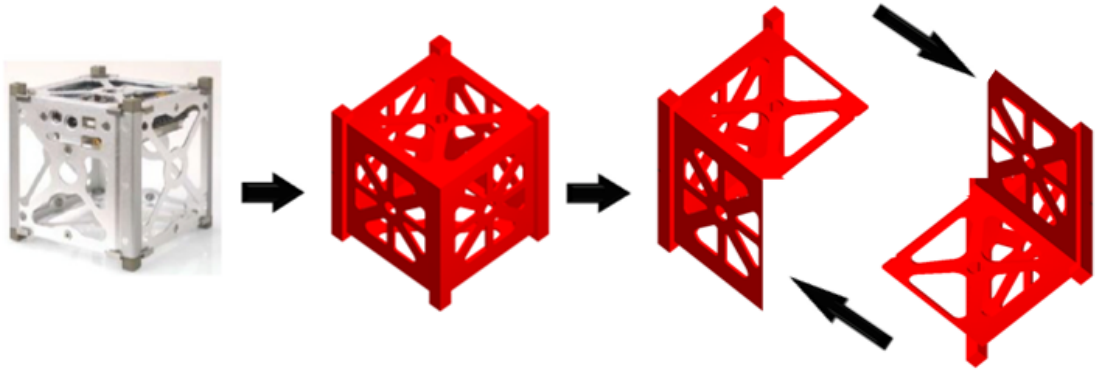

Traditional CubeSat AM CubeSat New design configuration

Figure 3.9 Design for AM logics on a traditional CubeSat.

AM applications were examined due to the potential benefits and future challenges in terms of the new structures in the space area. The potential advantages of AM in space devices is impressive in the fabrication stages, and more disruptive in the design step so like most space applications, highly complex geometry and lots of components are in play, and they need to have high performances, having possible customization and reduced weight, anticipating long term development and lots of changes in geometry and configuration before the final structure [31]. Figure 3.9 shows the traditional CubeSat and AM CubeSat which will be analyzed in section 3.4, and the new design configuration is an idea for the next step which is more ideal due to the capability of installing the inner components within the CubeSat.

3.3 Finite Element Analysis (FEA)

Time-dependent problems, according to the descriptions of physics in the space environment, are demonstrated as partial differential equations (PDEs). These kind of

equations (PDEs) in a variety of geometries and problems do not have any solutions with analytical techniques. Although some approximate equations can be defined according to different types of discretization methods, which approximate the PDEs with numerical equations. They can be solved by numerical methods and theses solutions are the real solution for the PDEs.

A method that uses a computational technique for obtaining numerical solutions of a variety of engineering problems is called the finite element method (FEM). The range of applications is from deformation and stress analysis of automotive, aerospace, building structures through to fluid flow related problems. Using FEM, complex problems can be solved by using computer-aided design (CAD) and can be modelled efficiently.

Before the fabrication of the prototype, several alternative shapes can be examined. The idea of FEM came from aircraft structural analysis and introduced a resolution of elasticity problems from the "framework method." In 1956, the stiffness matrices for truss and beam geometries were presented. Finally, the method of solving the stress analysis, transferring heat, and fluid flow problems were applied by engineers in the early 1960s [34]. The FEA approach has been used for solving complex engineering problems due to a lack of admissible and accurate analytical solutions. Some problems are complicated because of the complexity in terms of their geometries, loadings, and material properties. The approximate solutions in FEA are a numerical method to simulate the actual results in terms of predicting the behaviour of a part (or parts) under a given situation [34]. For modern simulation software, as the base, engineers are able to find the weak points, high-stress regions, etc. in their project.

3.3.1 Methods of Meshing

The computed simulation solutions for a specific problem needs to be carefully interpreted. For solving the mathematical problems, it is often beneficial to split up the problem into smaller, more tractable, ones. It is reasonable to solve the problem by multiple small pieces instead of the entire continuous domain [32].

It is possible analysis via a mesh generator and extracts all topological data and the model's geometry. At first, a coarse mesh is built, and then it is converted to a more optimized finite element mesh that incorporates the materials properties, load and analysis requirements [35].

A finite volume mesh is a standard for the operation of the mesh. This is often a three-dimensional, un-constructional mesh with two kinds of tetrahedral or hexahedral elements. In terms of the function of the shape, mesh elements can be defined as 1D, 2D and/or 3D elements (Figure 3.10).

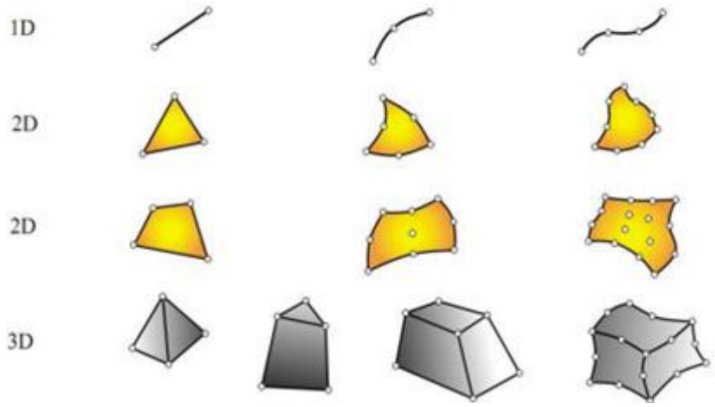

Figure 3.10 Mesh elements [32].

With respect to the accuracy and durability of FEA, the quality of the employed mesh plays a significant role. There are two kinds of 3D elements: tetrahedral elements with four nodes

and four faces, and hexahedral elements with eight nodes and six faces. By adding one node to each edge, the second-order elements have been created (Figure 3.11) [36].

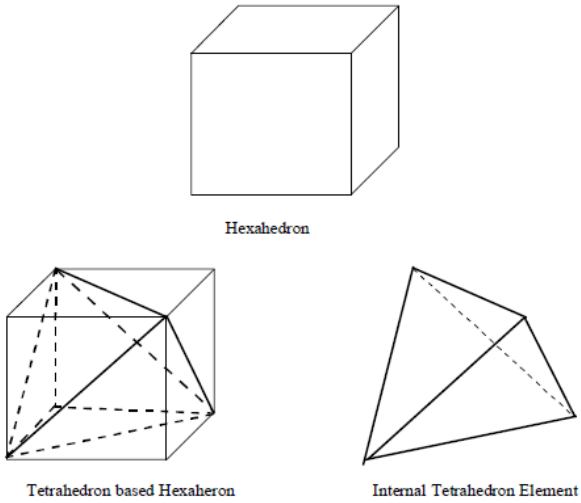

Figure 3.11 3D meshes [35].

The accuracy in hexahedral elements is greater than for tetrahedral elements. The second-order elements are accurate, due to having the approximate quadratic function instead of linear [36]. Some studies have been published to compare the convergence specifications of hexahedral meshes with tetrahedral one. The quadratic tetrahedral elements are equal with bilinear hexahedral elements according to the accuracy and processing time required [35]. A simple rectangular bar, with two kinds of tetrahedral and hexahedral meshes, is fixed at one side to show the comparison of linear and quadratic displacement. Figure 3.12 shows a simple bar with its geometry, boundary conditions and loading. In the static linear analysis, a load and a torsion are applied to the end of the cantilever beam, fixed its other end, for comparing the result of loads between hexahedron and tetrahedron meshes. Both of the displacement and bending stress are independent of Poisson's ratio [35].

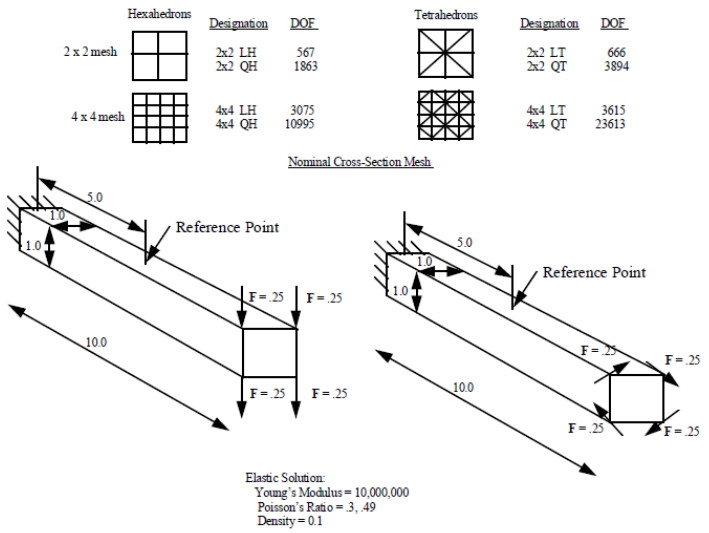

Figure 3.12 Static bending and torsional analysis [35].

Timoshenko and Goodier [37] presented the solution for displacement and the shear stress for the rotational problem. The below tables show the results of analytical solutions and computed by different finite element calculations.

Table 3-1 Displacement and stress errors in the bending model [35].

Bending	v= 0.3	Displacement			Bending	v = 0.3	Displacement		
DOF	LH	QH	LT	QT	DOF	LH	QH	LT	QT
561	0.72%				561	0.00%			
666			31.48%		666			21.23%	
1863		0.24%			1863		0.01%		
3075	0.08%				3075	0.00%			
3615			10.48%		3615			21.00%	
3894				0.24%	3894				0.33%
10995		0.01%			10995		0.01%		
23613				0.01%	23613				0.01%
Bending	v = 0.49	Displacement			Bending	v = 0.49	Displacement		
DOF	LH	QH	LT	QT	DOF	LH	QH	LT	QT
567	6.56%				567	0.01%			
666			71.66%		666			66.77%	
1863		5.36%			1863		0.01%		
3075	3.2%				3075	0.01%			
3615			44.8%		3615			35.23%	
3894				4.80%	3894				0.01%
10995		2.88%			10995		0.01%		
23643				2.48%	23613				0.23%

The tables show that the maximum errors are produced by the linear tetrahedron element (LT).

Table 3-2 Displacement and stress errors in torsion [35].

Bending	v= 0.3	Displacement			Bending	v = 0.3	Displacement		
DOF	LH	QH	LT	QT	DOF	LH	QH	LT	QT
561	15.65%				561	37.59%			
666			50.81%		666			77.82%	
1863		1.99%			1863		7.97%		
3075	5.26%				3075	8.59%			
3615			22.39%		3615			38.40%	
3894				3.23%	3894				0.07%
10995		0.49%			10995		0.01%		
23613				0.76%	23613				0.01%
Bending	v = 0.49	Displacement			Bending	v = 0.49	Displacement		
DOF	LH	QH	LT	QT	DOF	LH	QH	LT	QT
567	26.41%				567	26.41%			
666			68.80%		666			68.80%	
1863		2.60%			1863		2.60%		
3075	5.44%				3075	5.44%			
3615			52.72%		3615			52.72%	
3894				4.80%	3894				4.7%
10995		0.75%			10995		0.75%		
23643				1.41%	23613				1.41%

In terms of comparing the accuracy of all tetrahedral meshes to all hexahedral meshes, it shows that with linear tetrahedrons the stiffness matrix eigenvalues are more extensive than for the linear hexahedrons, which means the linear hexahedrons can deform with lower strain energy; consequently, it is more accurate. Linear tetrahedron element (LT) models in linear static bending have an error between 10 to 70 percent in both displacement and stress computation, which is not acceptable. However, models with linear hexahedron (LH), quadratic hexahedron (QH) and quadratic tetrahedron (QT) meshes provided acceptable results [33].

3.3.2 CubeSat Structure

3.2.2.1 Geometry

The weight and physical size are the two distinct characteristics of CubeSats. For a 1U (unit) standard CubeSat, the weight is less than 1.33 kg, and its size is a 10 cm cube, approximately [33]. Satellite designers need to have envisioned structures to provide flexibility during the design, improvement, and examination stages, especially for allowing

changes in the structure without redesigning the subsystem(s) in the main structure. The three requirements for designing the CubeSat are:

1- a system of deployment and associated launch vehicle,

2- a standard specification of the CubeSat geometry/parameters,

3- the compatibility of materials for use in space/launch scenarios.

To reach the final model of design, the structure needs to go through several phases. The flowchart in Figure 3.13 shows the design in all phases. The chart shows that after the initial finite element design, any design failing to fulfill the launch requirements returns to the design phase [38].

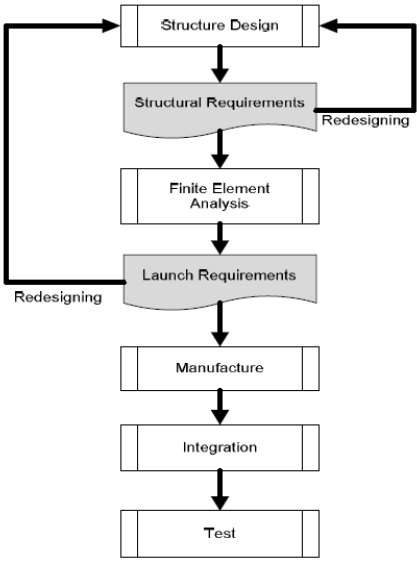

Figure 3.13 Flowchart of design [38].

The other critical step for design is predicting the forces that are applied to the CubeSat from the launch. A small inaccuracy in finite element design comes from the complexity and a variety of mission environments that can, potentially, cause significant errors. Various external loads are applied to a satellite during its launch: (i) booster acceleration, (ii) air turbulence, (iii) engine vibration, (iv) ignition and burn out of the booster, etc. From

launch to orbit, every event produces structural loads on a spacecraft, which may impact its useful life.

A 1U CubeSat, shown in Figure 3.14, is designed using the NISA software. The size of CubeSat is 10x10x10 cm with a 2 mm thickness.

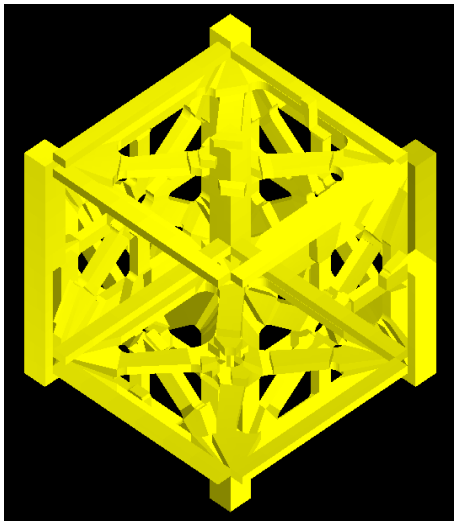

Figure 3.14 Structural geometry of the 1U CubeSat in this study.

3.3.2.2 Material

One of the significant aspects of space manufacturing is choosing the material in designing the structure of the satellite. Weight, strength, stiffness, thermal conductivity, thermal expansion and expense are important factors for designing the CubeSat. In the space environment, material requirements are:

1- The material should be in the list of NASA materials,

2- The selected material's thermal expansion coefficient and that of the deployment system should be similar,

3- The von Mises stress should be less than the yield strength of the selected material,

4- The material should be able to be manufactured by the selected method (e.g., machining or, potentially, 3D printing),

5- Materials with the low density are acceptable,

6- The materials should have low out-gassing property.

Currently, the available lightweight materials for the SLM method are selected titanium and aluminum alloys. High purity Ti (known as commercially pure, or CP-Ti) and Ti-6Al-4V (Ti64) are used for aerospace and biomedical properties, and use has been expanded due to their high strength to weight ratio and excellent corrosion resistance and fatigue characteristics.

Magnesium alloys also are another class of lightweight metals that have been used in many industries that needs to reduce the weight significantly. Magnesium alloys has a stiffness double to that of to bone, with the advantage of minimizing the harmful effects of stress shielding [39]. The alloy was first used in biomedical applications in the last 18^{th} century and have an history for use in aircraft manufacturing and are thus alloys used for some recent initiatives [40].

Additive manufacturing (AM) of Mg alloys is increasing and is a potential replacement for traditional manufacturing when fabricating complex designs. Magnesium, with a highly reactive nature, is known as a difficult metal for use in 3D printers. The pure form of magnesium oxidizes uncontrollably and in AM method raw material are typically required in powder form. Consequently, the metal's surface energy grows and causes reaction with oxygen in the atmosphere to provide combustion [39]. In addition, recent investigation shows because of the low vaporizing temperature, fabricating three-dimensional magnesium parts has not led to a possible operation yet [41].

Aluminum alloys are the materials which are receiving attention from researchers in terms of manufacturing by AM. Large number of applications in automotive and aerospace

industries have been using Aluminum and Aluminum alloys. The number of processable Al alloys are still quite limited due to having some challenges during the SLM with laser-melting aluminum [42].

Al-Si alloys are the most investigated Al alloys, with high fluidity, high weldability, corrosion resistance and low thermal expansion coefficient [43]. An abundance of published works has been completed on optimizing Al alloys to eliminate the formation of defects such as cracks, pores, distortions, etc. in manufactured parts. Some of these weaknesses are solved, but others still need post-processing. Ultimately, by using a range of SLM, it is possible to fabricate defect-free parts from Al-Si [44]. For the time being, AlSi10Mg and AlSi12 are the most commonly used aluminum alloys in AM [45] [44]. In Table 3-3 there are mechanical properties of AlSi12 and AlSi10Mg alloys.

Table 3-3 Properties of the aluminum alloys (AlSi12 and AlSi10Mg) [46].

Material property		Magnitude
AlSi12	Elastic Modulus	72-77 GPa
	Yield Strength	230×10^6 Pa
	Poisson's Ratio	0.32
AlSi10Mg	Elastic Modulus	70 GPa
	Yield Strength	230×10^6 Pa
	Poisson's Ratio	0.33

In Table 3-4 the mechanical properties of AlSi12 and AlSi10Mg produced by AM technology is shown and all simulations in part 3-4 are calculated by these properties. For comparative purposes, they will both be applied to the designed CubeSat and will be analyzed, which will be demonstrated in part 3.3.1.1.

Table 3-4 Properties of aluminum alloys fabricated by AM (AlSi12 and AlSi10Mg) [26] [47].

Material property		Magnitude
AlSi12	Elastic Modulus	75 GPa
	Yield Strength	260×10^6 Pa
	Poisson's Ratio	0.3
AlSi10Mg	Elastic Modulus	72 GPa
	Yield Strength	170×10^6 Pa
	Poisson's Ratio	0.3

3.3.2.3 Other Requirements

After the material selection, it is important to determine the von Mises stress under the static loads; a first design should thus be obtained and analyzed. Figure 3.15 shows the 3U CubeSat loading condition (gravity load) [36].

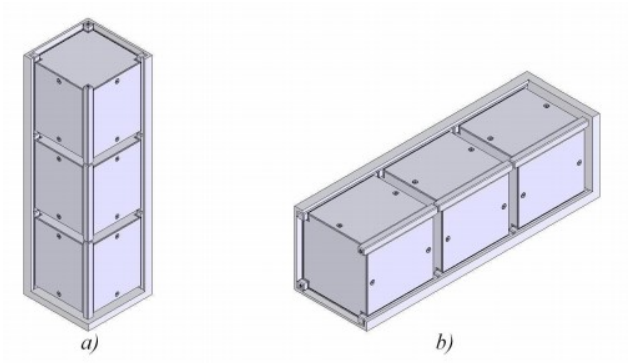

Figure 3.15: a) Vertical sequence, and b) Horizontal sequence [36]. .

A first design should be obtained and analyzed, after initially selecting the chassis material. Finite element analysis can then be performed to the maximum stress, in terms of static loads on the design. The first design on an assembled and exploded 1U CubeSat is shown in Figure 3.16 [48].

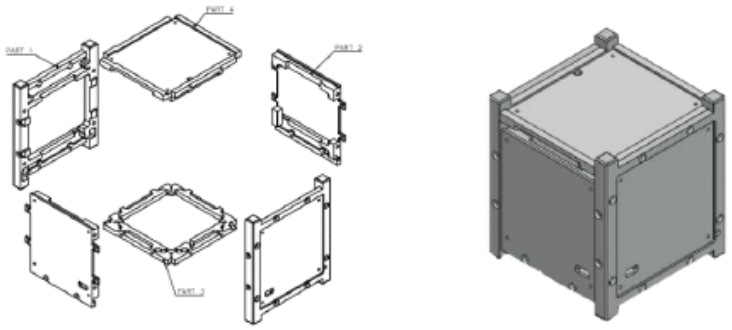

Figure 3.16 Design of 1U CubeSat (Surya Satellite Structure) [36].

For solving the finite element equations or set of differential equations, boundary conditions need to be satisfied (Figure 3.17). Defining the boundary condition is the most critical aspect in finite element design. To analyze the CubeSat, the boundary condition, according to the figures below, has been considered.

Color	u_x	u_y	u_z
	0	0	0
	Free	Free	0
	Free	Free	Free
	0	Free	Free
	Free	0	Free

Figure 3.17 Applied constraints on a CubeSat [49].

During the launch, the CubeSat is located in the deployer, and it is allowed to move among the deployer's rails, on its own rails (Figure 3.18 and Figure 3.19). As shown in the below figures, only one rail end in the Cube is restrained in three directions, which is marked in red [49].

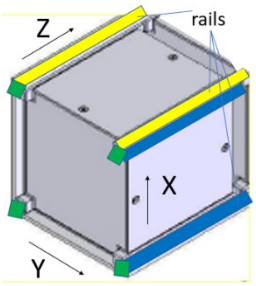

Figure 3.18 View from the bottom.

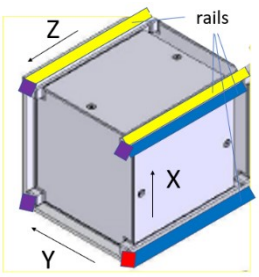

Figure 3.19 View from the top.

Table 3-5 shows the whole CubeSat's load, with a quasi-static load related to the maximum acceleration in three directions.

Table 3-5 Quasi-static loads.

Global coordinate	Acceleration (G)
X direction	+/- 7
Y direction	+/- 4
Z direction	+/- 4

In addition, the frequency's limitation is 20 to 2000 (Hz).

The capability of withstanding in the thermal environment in space is another of the requirements for a CubeSat design. The table below shows the expected mission's thermal environments and also the solar loading conditions, -60 and 73 degrees, as defined in Table 2-3.

3.4 Results in NISA

There are two types of analysis for the mechanical parts, the static and dynamic analysis, which play an important role for the performance and accuracy of the function performed by design engineers. The purpose of these types of analysis are estimating the behaviour of the mechanical parts under the operational conditions. In this specific study the analysis is static, due to having the constant loads on the structure. In this part, the linear stress

analysis, deformation analysis and thermal analysis will be illustrated. However, in a dynamic modal analysis, its vibration modes would be identified. Both of the analyses will be described for two geometries with different thicknesses.

3.4.1 Wall thickness of 2mm

The CubeSat was designed as geometry with a 2 mm thickness in its six faces. Then it is loaded with a quasi-static load according to information provided in Table 3-5. Figure 3.20 shows the defined mesh which has been created by using hexahedral elements.

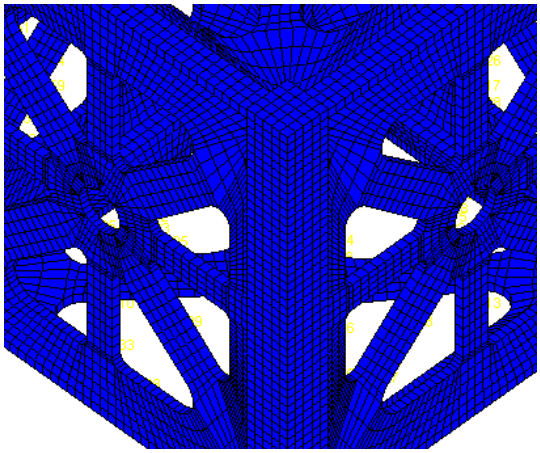

Figure 3.20 Hexahedral elements in CubeSat.

3.4.1.1 Stress in the CubeSat

AlSi10Mg:

In order for a CubeSat to survive, all of the accelerations in three directions, according to Table 3-5, should apply simultaneously. If the maximum stress is less than the yield strength of AlSi10Mg ($\sigma_{yield} \approx 170 \times 10^6$ Pa), the CubeSat could withstand the environment. This analysis is linear due to having linear relation between the applied loads and displacement, it is also analyzed under the explicit analysis to get the results rapidly in this complex shape and the whole analysis is conducted by NISA software. This example illustrates the maximum von Mises stress of 809.3×10^2 Pa, which is less than the yield

stress, 170 × 10^6 Pa. The result of von Mises stress in the global coordinate system is shown in Figure 3.21:

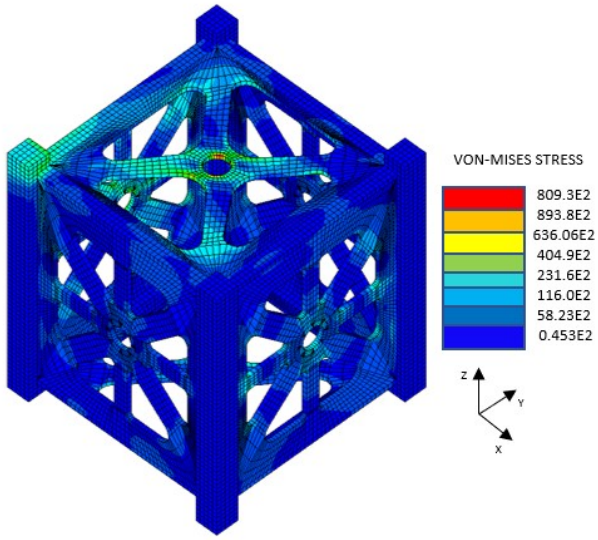

Figure 3.21 Von Mises stress distribution under the overall accelerations with 2 mm (AlSi10Mg).

In addition, this result was not changed after applying solar loading conditions. The temperature variation or a temperature difference of 133 °C (solar thermal loading temperature range: -60 °C and 73 °C) is viewed as the absolute extreme scenario, and actual temperature variation will be significantly less [50]. In this part factor of safety can shows the strength of the designed CubeSat with AlSi10Mg, which can be calculated by dividing the yield strength of AlSi10Mg to the maximum calculated stress (von Mises stress): FOS $= \frac{\sigma_{yield}}{\sigma \mathrm{vm}} = \frac{170 \times 10^6}{809.3 \times 10^2} = 2101$

The huge value of FOS is preferred due to ignoring the random vibration. The von Mises stress which is calculated in this FOS is obtained only by applying acceleration simultaneously. But random vibration, like acceleration, produces stress which is much

larger than the von Mises stress by acceleration. Consequently, if the total stress is input into the FOS equation, the results would be much smaller.

AlSi12:

In this section the material is changed to AlSi12 to analyze and compare with the AlSi10Mg. The condition of analysis and the yield strength of AlSi12 is ($\sigma_{yield} \approx 260 \times 10^6$ Pa), similar with AlSi10Mg. The result of maximum von Mises stress is 810.8×10^2 Pa

(Figure 3.22). So, the FOS for this material would be: $\text{FOS} = \frac{\sigma_{yield}}{\sigma\text{vm}} = \frac{260\times10^6}{810.8\times10^2} = 3209.$

The huge value of FOS in AlSi12 arises from the same reason which is explained above for AlSi10Mg.

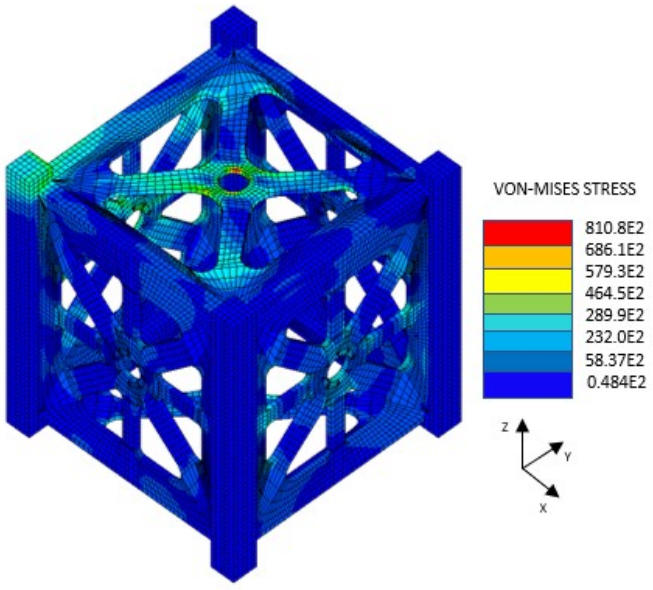

Figure 3.22 Von Mises stress distribution under the overall accelerations with 2 mm (AlSi12).

Due to having a lower value of the maximum von Mises stress with material AlSi10Mg in comparison with AlSi12, the rest of the simulations would be illustrated for AlSi10Mg configuration.

3.4.1.2 Deformation of the CubeSat

Below, in Figure 3.23, the result shows the deformation in the top face of the CubeSat with exaggeration of scale in the Z direction after applying all of the accelerations in three directions, according to Table 3-4, simultaneously.

Figure 3.23 Deformation of the top plate in the z-direction.

The result of the maximum displacement in the z-direction is 73×10^{-9} (m), which occurs in the center of the top and bottom face of the CubeSat, and it is minimal on the columns and the other faces (Figure 3.24).

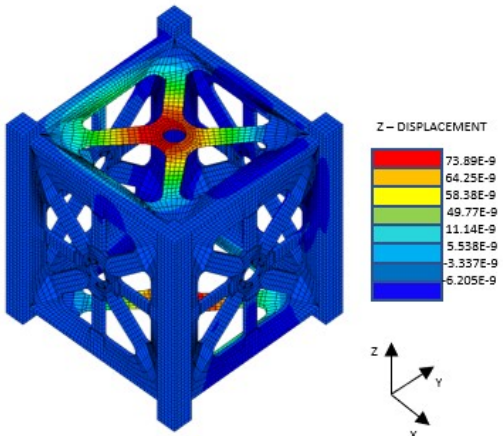

Figure 3.24 3D Displaced shape in the z-direction in (m).

The displacement in the y-direction and x-directions are 84.23×10^{-9} (m) and 75.89×10^{-9} (m), respectively (Figure 3.25). These displacements are more than the z-direction value, due to the restriction of the rails in both the x- and y-directions.

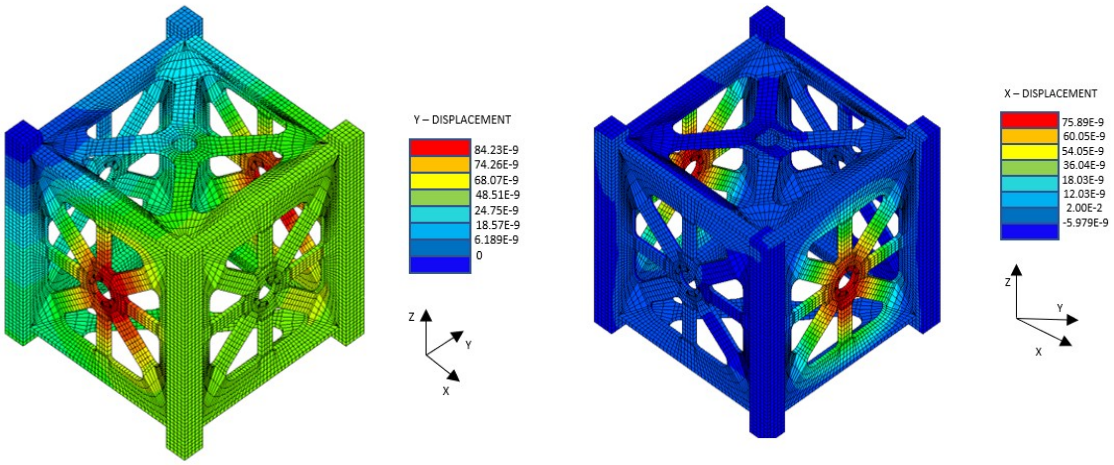

Figure 3.25 3D Displaced shape in the Y direction (left) and X direction (right) in (m).

Figure 3.26 shows the final displacement and deformation in all directions, simultaneously.

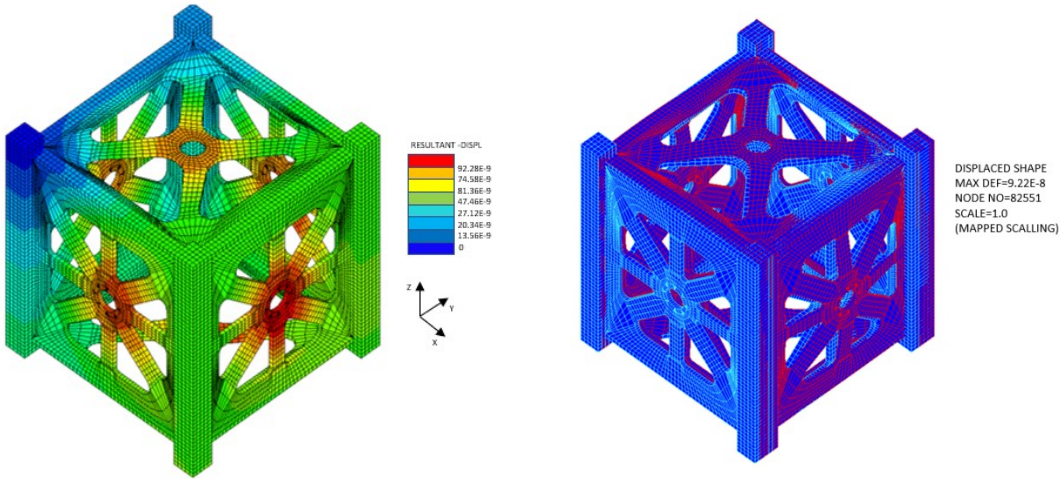

Figure 3.26 Overall displacements (left) and maximum deformations (right).

3.4.1.3 Modal analysis

This analysis characterizes the results of the dynamic action on the CubeSat under dynamic forces. The natural frequency threshold is the prominent characteristic of space constructions like the CubeSat; so, in the structure, the first natural frequency must be more than a specific quantity specified for the launch vehicle. The typical range of this value is

from 50 to 90 Hz [2]. Figure 3.27 shows the first four modes of frequencies. The natural frequencies result from mode one to mode four are 1432, 1447, 1449, and 1898 Hz, respectively.

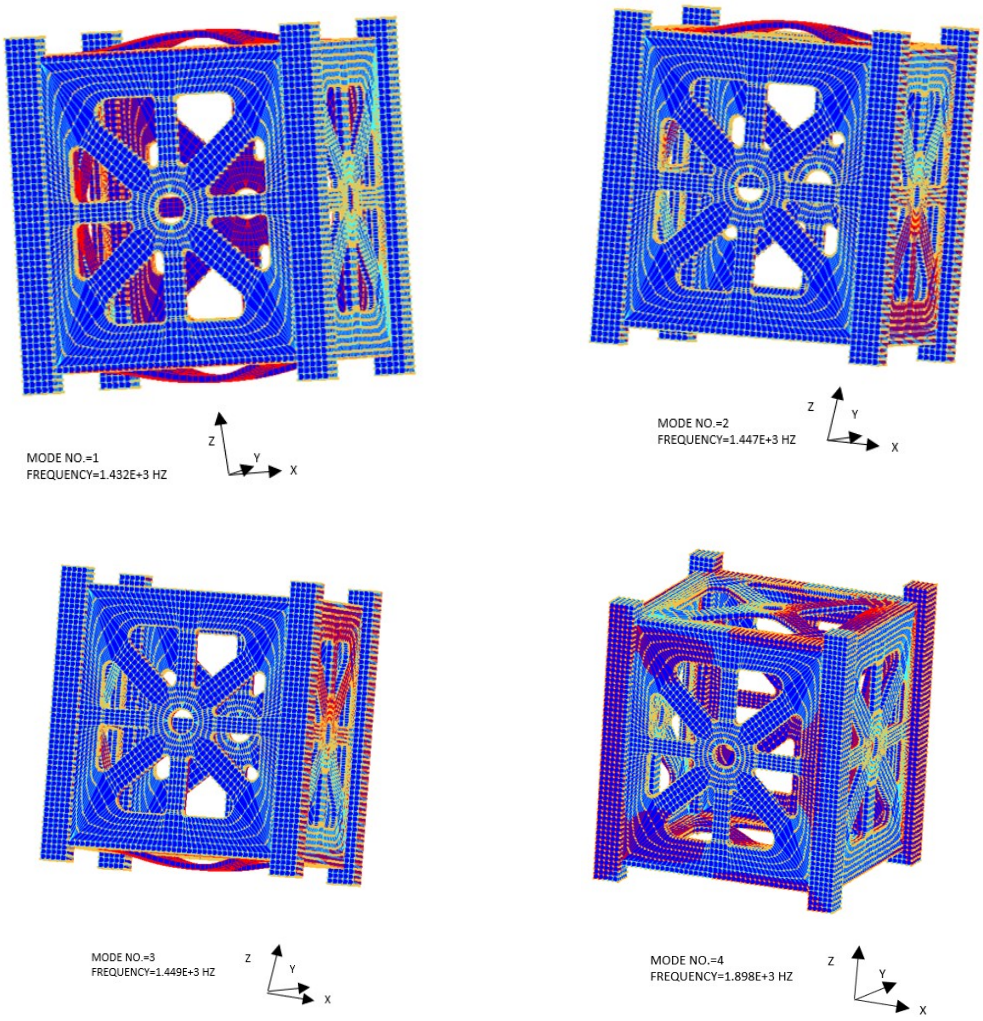

Figure 3.27 The first four natural frequencies and mode shapes for IU CubeSat (2 mm width).

3.4.2 Thickness of 4 mm

The CubeSat has also been created with the faces having 4 mm wall thickness and a quasi-static load following maximum longitudinal and lateral acceleration, as outlined in Table 3-5. The CubeSat with 4 mm thickness has been created to compare with the CubeSat (2 mm wall) in the results of stress, displacement, deformation, mass, etc.

3.4.2.1 Stress in the cube

The maximum calculated von Mises stress in this simulation determined using NISA was 302×10^2 Pa, less than the one in the Cube with 2 mm thickness, indicating this is stronger geometry. However, by increasing the thickness, the weight of the CubeSat increases which is a negative factor in the CubeSat's requirements.

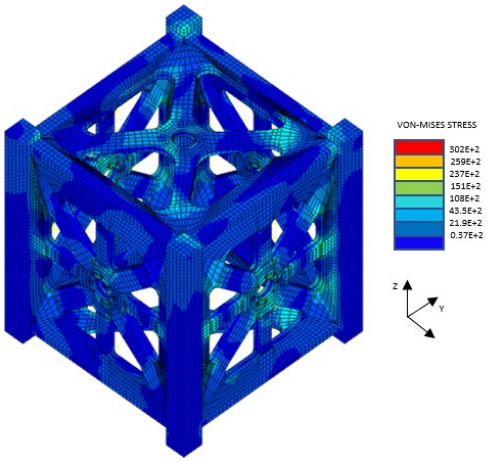

Figure 3.28 Von Mises stress under the overall acceleration with 4 mm.

The result of the von Mises analysis after applying the thermal conditions did not change, as was seen in the model with a 2 mm wall thickness.

3.4.2.2 Deformation of the CubeSat

The deformation of the model has the same pattern which was seen in Figure 3.23. The maximum displacement in the z-direction with 4 mm wall thickness was determined to be 20×10^{-9} (m). A comparison with the previous results (2 mm width) shows the displacement results in the CubeSat with a 2 mm wall thickness is three times greater than the 4 mm geometry.

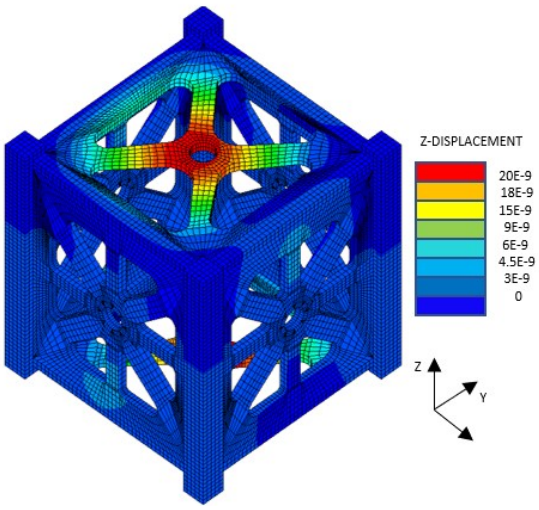

Figure 3.29 Displacement in the z-direction.

The below figures show the displacements in the x- and y-directions. The results show more deformation in the x- and y-directions than the z-direction, due to the BCs and the values accelerations.

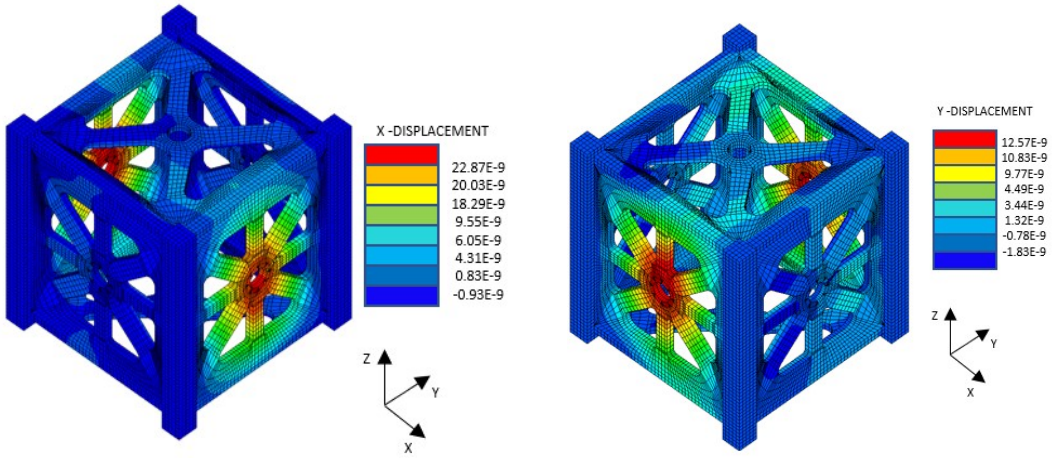

Figure 3.30 3D displaced shape in the x-direction (left) and y-direction. (right).

Finally, Figure 3.31 shows the displacements and deformations in all directions.

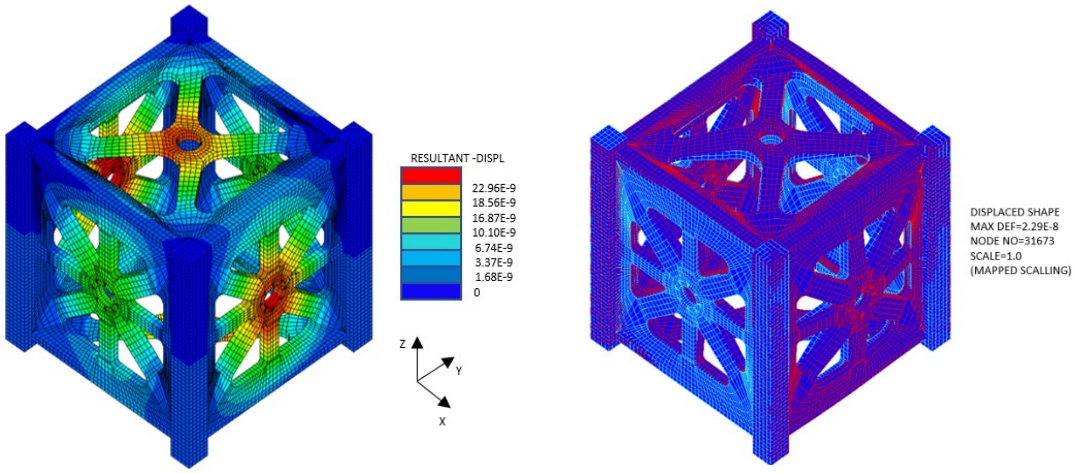

Figure 3.31 Overall displacements contours (left) and maximum deformation (right).

The results of FEA performed using NISA for the two different models are summarised in Table 3-5.

Table 3-6 Results of FEA analysis by NISA.

Thickness	Material (AM)	von Mises stress (Pa)	Yield Strength (Pa)	Mass (kg)	Volume (m^3)	Safety factor
2 (mm)	AliSi10Mg	809.3×10^2	170×10^6	0.289	1.08×10^{-4}	2101
2 (mm)	AlSi12	810.9×10^2	260×10^6	0.289	1.07×10^{-4}	3206
4 (mm)	AliSi10Mg	302×10^2	170×10^6	0.458	1.71×10^{-4}	5623

The mechanical properties of the AlSi10Mg and AlSi12 CubeSats, in Table 3-6, produced by the AM technology.

3.4.2.3 Modal analysis

In this analysis, the dynamic behaviour of a CubeSat with 4 mm thickness, under dynamic loads, is illustrated. Figure 3.32 demonstrates the natural frequencies of the first 4 modes. The natural frequencies for these modes are 2800, 2812, 3484, and 3544 Hz, respectively.

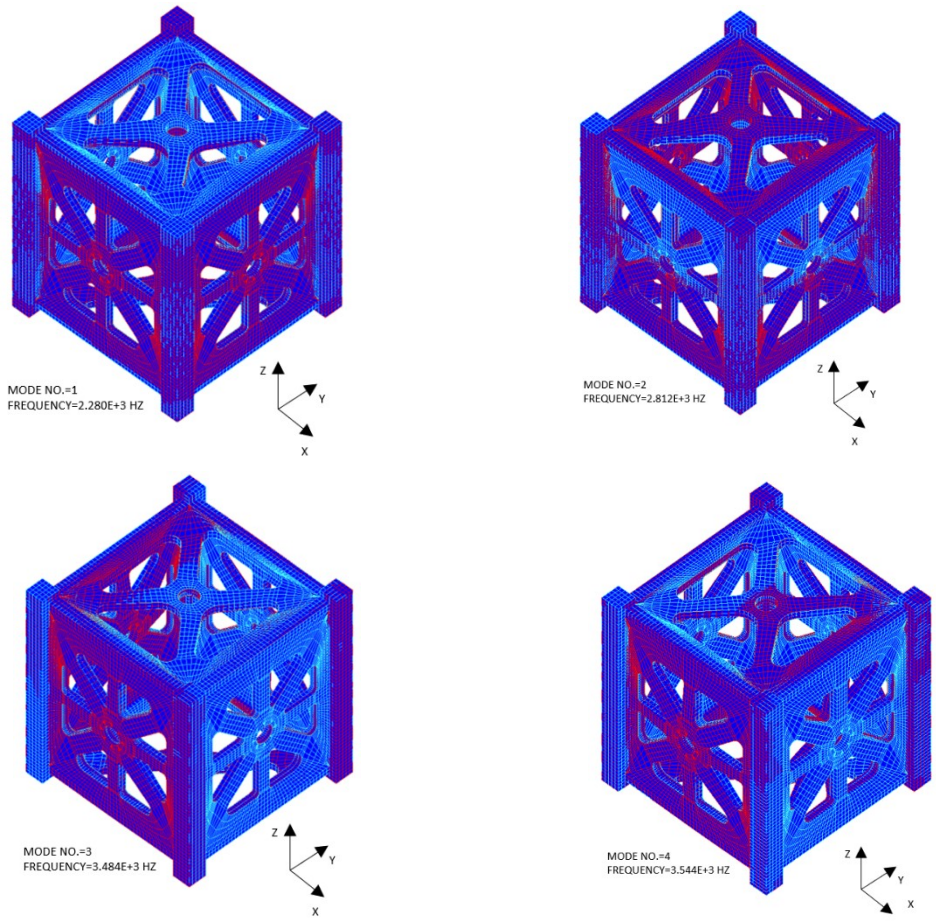

Figure 3.32 The first 4 eigenvalues and mode shapes for IU CubeSat (4 mm width).

3.4.3 Discussion

All the simulations have illustrated the structurally sensitive areas after finalizing the shape of the CubeSat and its material, allowing the possibility to adjust the design of aluminum CubeSat accordingly. The maximum von Mises stress values are less than the yield strength of AlSi10Mg, and it shows the acceptable reason for using this material in terms of its design. The deformation values also play a crucial role in accepting the shape of the design, and its material. The results in Table 3-6 indicate that the CubeSat will withstand use for both designs, although obviously, the thinner wall results in greater mass saving. The value of the applied loads was the highest that might be predicted for launch scenarios, so this

result is a conservative approach. In addition, the calculated mass of both Cubes is significantly less than 1 kg, which is an important factor for accepting this layout of 1U CubeSat. The last part to confirm the feasibility of both designs of the CubeSats is the CubeSat's natural frequencies being above the mission specified values.

CHAPTER 4 INVESTIGATION AND VALIDATION

One of the verification methods that will always be utilized in satellite design is doing a series of validation tests. Two types of testing can be readily done for a CubeSat: internal and verification testing. The first one is completed based on the operational purpose of the satellite, but the verification testing consists of thermal and vibration tests. Therefore, these tests help to realize different development stages of the satellite, through the life cycle of a project: acceptance, capability, and during the launch or in orbit; elements of the equipment; in different types of testing, engineering, structural, thermal and others. Below the most used tests are illustrated in more detail [51].

4.1 Functional Testing

Checking the satellite in terms of being able to perform all of the programmed duties properly, against its software design and operation, is viewed as a functional test [7]. Functional tests are focused upon the basic mission, with the aim of guaranteeing the survivability of the satellite, such as communications, power distributions, and defect handling. Due to the lack of a suitable environment to simulate space situations on the earth, a variety of tasks such as orbital positioning and attitude control cannot be readily quantified. So, as a consequence, having a complete verification of orbital function is inevitable. Functional tests are applied before and after all main tests, in order to check operation and potentially improve the satellite, [7].

4.2 Thermal

A successful mission in the harsh environment of space can potentially be guaranteed by proper thermal design and its testing/validation [20], along with the functional tests outlined previously. For testing the thermal campaign, a thermal-vacuum facility has been necessary [2]. The thermal-vacuum is the favoured environment to verify the effectiveness of the thermal design of a CubeSat [40]. This chamber can provide the environment needs in terms of the vacuum and temperature conditions for completing the thermal cycling tests and thermal bake-out, which are the two different tests that are typically required. In thermal cycling, different temperatures are applied in different cycles, to simulate the space conditions. In the thermal bake out test, the mass loss of satellite is evaluated to assess potential outgassing, and this should not be more than 1% of the whole mass in the satellite [2].

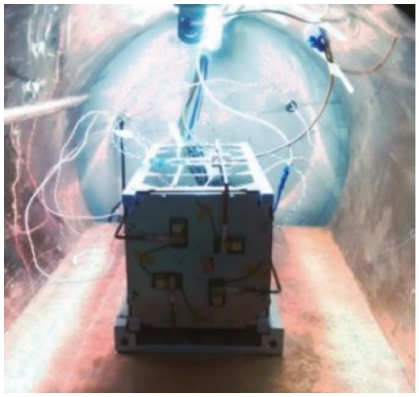

Figure 4.1 Thermal vacuum chamber [2].

4.3 Vibration

Shock and vibration are the two common kinds of dynamic testing that are applied for satellite design. Although the vibration test is necessary for all launches, shock testing is

not always required [14]. The engineering vibration testing is divided into harmonic vibration (subject to sine wave) and random vibration testing. For understanding the natural vibration of any structure, harmonic vibration testing could help. A vehicle on a road, the wings of an airplane in turbulent air flows and deploying a CubeSat are subjected to vibrations which are not repetitive and predictable like a harmonic vibration. The main objective of testing the random vibration in industry is to subject a Device Under Time (DST) to failure. For environmental vibration, random vibration testing would be the best option due to being more realistic than sine testing. But the application of this test is not perfect, while it still needs to be used in some form in qualification procedures [52].

Figure 4.2 shows an electromechanical shaker table, and the satellite, in order to carry out vibration tests in the z-direction [14]. For performing vibration in different directions, the shaker table/satellite orientation must be rotated 90 degrees in the x- and y-directions.

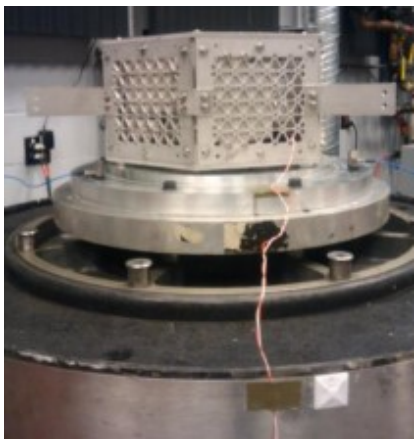

Figure 4.2 Kind of CubeSat mounted to the shaker table [14].

Also, the natural frequency of the space structures, such as a CubeSat, is one of the major modal characteristics; the first natural frequency, which is usually defined by the launch carrier, must be greater than a particular quantity and it is mentioned in 3.3.1.3 [2].

.

4.3.1 Test requirements

Years of preparation are required for satellite development projects. Having a sufficient safety margin for spacecraft is crucial to dimensional stability and sustained loading circumstances during the launch time. In each launch step the load contribution must be defined for design purposes. There is a combination of two load cases for CubeSat structure, which is listed in Table 4-1 [49].

Table 4-1 Load combination.

Load case 1	Random vibration	Level of NASA qualification
	Acceleration	Longitudinal 7G Lateral 4G
Load case 2	Shock	The 1st payload on side of P-POD

The value of stress (σ_{VM}) used for calculating the safety factor for load case 1 is the sum of the stress extracted from random vibration analysis and the stress from the quasi-static loading, which is deterministic. In load case 1 only the maximum von Mises stress value is taken into account for calculating the safety factor. The operation of engine as well as noise generated by satellite produces the random vibration, which causes significant stress state. As the von Misses stress caused by random vibration has not been taken into account in calculation of safety factor in this thesis, as a result a high safety factor has been produced. In other words, considering the summation of acceleration and random vibration loads would produce higher von Mises stress and therefore a lower SOF [49].

CHAPTER 5 SIMULATION RESULTS (FEA) AND COMPARISON WITH THE CURRENT RESULTS

5.1 The UWE-4

In 1999, California Polytechnic State University (CalPoly) drafted the first CubeSat Design Specifications (CDS). This study aims to create a more efficient and straightforward (1U) CubeSat and analyze it under the mentioned criteria in its journey to the low earth orbit in space during the launch. In Chapter 3, the output of the software proves the CubeSat's design stability; however, in the validation process, the comparison of the present study with another current research can also be performed. The mechanical requirements in the CDS are:

1- Similarity of thermal expansion in the CubeSat material and the deployer material (Al 7075).

2- Having smooth, flat and hard anodized rails in order to minimize friction and/or preventing cold welding from the launch conditions, especially during release from the deployer

3- Tolerances in the design of CubeSat are based on PD specifications

The UWE-4 is a CubeSat that is designed in CAD and it is considered to be simpler and more efficient. This CubeSat is also compared with its previous version, in terms of being more accurate in fabrication. In this study for doing FEA, the actual model is completed by SolidWorks to import to NX for completion of the final analysis [53].

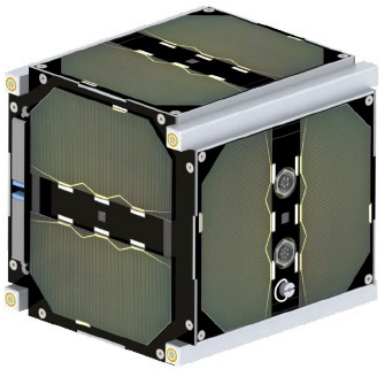

Figure 5.1 Anatomy of UWE-4.

Figure 5.1 is a subsystem containing:

1- Communication system,

2- OBDH (Onboard Data Handling),

3- ADCS (Attitude Determination and Control System),

4- Batteries, screws, spacers,

5- PPU (Power Processing Unit) and Thruster (if needed).

The comparison should be started from the design of the CubeSat until the achievement of the results from software evaluation, although some of the conditions may not be similar during the respective journeys of two CubeSats (or their construction materials), which consequently may lead to some differences between the results. Figure 5-1 shows the technical drawing of the 1U CubeSat in this study, and Figure 5.2 shows the initial design of UWE-4.

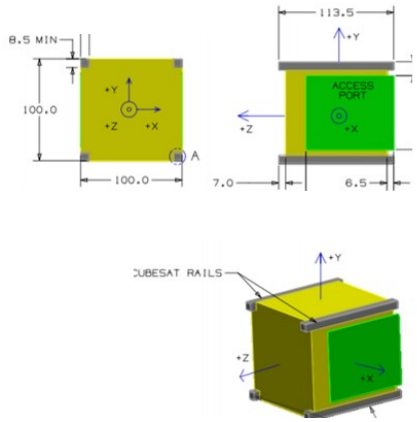

Figure 5.2 Drawing of 1U CubeSat specification [53].

There are small differences in the size of the columns and the total length of CubeSat in the z-direction (1.5 mm) in comparison with the CubeSat which is completed in Chapter 3 (Figure 5.3). It should be noted that the design of a CubeSat can be affected by the shape of the PD.

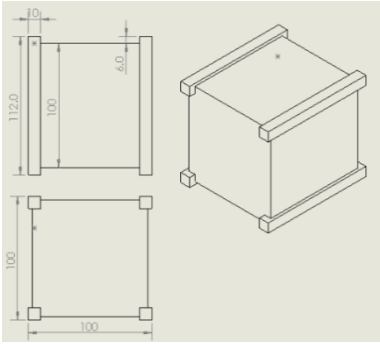

Figure 5.3 1U CubeSat design in this study.

The next step in the process of modelling is managing the properties for all components. The characteristics of nodes and elements can be defined in terms of the material properties in the FEM. The material properties for this CubeSat are listed in Table 5-1.

Table 5-1 Material properties.

Material	Density ($\frac{kg}{m^3}$)	Young's Modulus (GPA)	Poisson's Ratio	Yield Strength (MPa)
Aluminum Alloy (Al6061-T6)	2711	68.9	0.33	276

For getting the accurate design in FEA, around the location of holes, the specific shape of elements, spider meshes, (which are shown in Figure 5.4) can be used. These regions have more stress during loading.

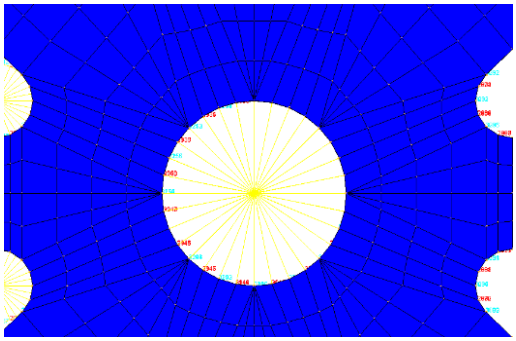

Figure 5.4 Mesh representation around the holes (spider mesh) [53].

Figure 5.5 shows the FEM of UWE-4 CubeSat.

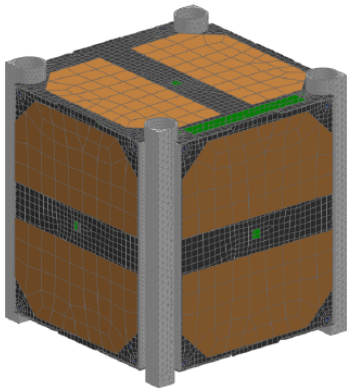

Figure 5.5 FEM mesh of UWE-4 CubeSat [53].

In this CubeSat, like the CubeSat design, which is developed in Chapter 3, the static, dynamic, vibration, and loads were applied for simulating the exact conditions of the

system. In the UWE-4 the maximum static acceleration in the longitudinal direction is 10.5g, and in the lateral direction, the maximum acceleration is 3.5g. The mentioned acceleration values are provided by ISILaunch Services (the service with the aim of making the launch of simple satellites easier and simpler). In the present CubeSat, in terms of the horizontal arrangement, the load for a CubeSat with 1.33 kg mass would be 137 N (10.5g × 1.33kg = 137) arrangements of the combined loads are shown in Table 5-2.

Table 5-2 Scenarios of possible loads

Vertical Loading arrangement		
Major loading vector	Lateral loading direction	
Z+	X-	Y-
	X+	Y-
	X+	Y+
	X-	Y+
Z-	X-	Y+
	X-	Y-
	X+	Y-
	X+	Y+

Vertical Loading arrangement		
Major Loading vector	Lateral loading direction	
X+	Y+	Z+
	Y-	Z+
	Y+	Z-
	Y-	Z-
X-	Y+	Z+
	Y-	Z+
	Y+	Z-
	Y-	Z-
Y+	X+	Z+
	X-	Z+
	X+	Z-
	X-	Z-
Y-	X+	Z+
	X-	Z+
	X+	Z-
	X-	Z-

Operating temperature limitation is different for onboard components and it depends on the functions. The below table shows various components with their operating temperature ranges.

Table 5-3 Temperature of component's operation.

Components	Notes	Operating Temperature	
		$T_{min}[^\circ C]$	$T_{max}[^\circ C]$
Li Po Battery	(charge)	0	+45
	(discharge)	-20	+60
Solar Cells		-40	+125
Electronics		-40	+85
Main Structures		-40	+85

This model is simulated in a vertical-horizontal arrangement and the normal forces are applied to the contact areas (rails) on the CubeSat. Figure 5.6 shows the vertical arrangement of case 1 according to Table 5-4.

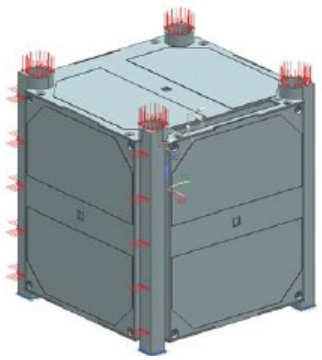

Figure 5.6 Normal forces in vertical arrangement [53].

For static analysis, the displacement and von Mises stress in various scenarios for the vertical arrangement is summarised in the below table. Each scenario contains the geometrically distributed normal forces on the rails of CubeSat.

Table 5-4 Displacement and maximum von Mises stress in a vertical arrangement.

Case	Scenario	Longitudinal Axis (10.5g)	Transversal Axis (3.4g)	Maximum Displacement (mm)	Maximum von Mises Stress (MPa)
1	Z+	X-	Y-	0.184	51.19
2		X+	Y-	0.135	54.88
3		X+	Y+	0.0731	40.06
4		X-	Y+	0.162	41.02
5	Z-	X-	Y+	0.0708	19.77
6		X-	Y-	0.0871	16.32
7		X+	Y-	0.0595	18.79
8		X+	Y+	0.0673	22.92

The figure below shows case 3 of the value of the maximum displacement of CubeSat in NX (Figure 5.7).

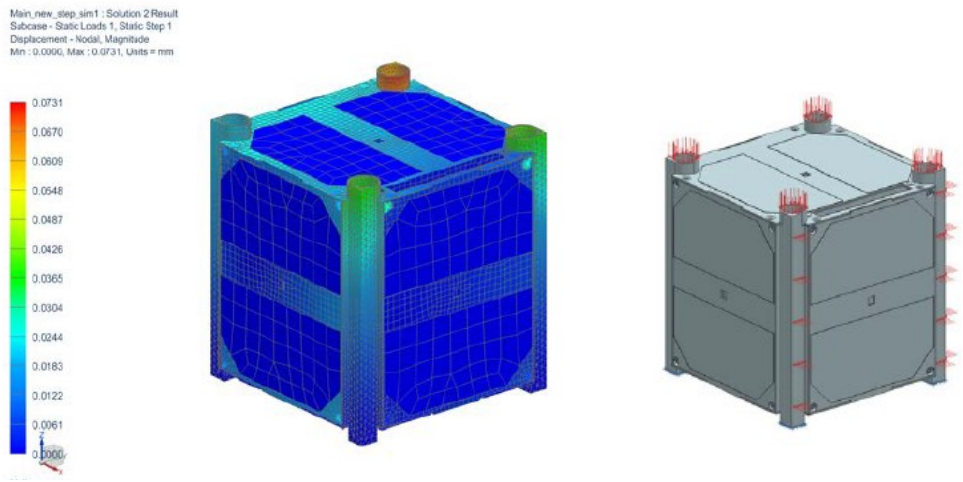

Figure 5.7 Maximum displacement in case 3 (mm).

The region where the maximum von Mises stress occurs in UWE-4 is shown in Figure 5.8.

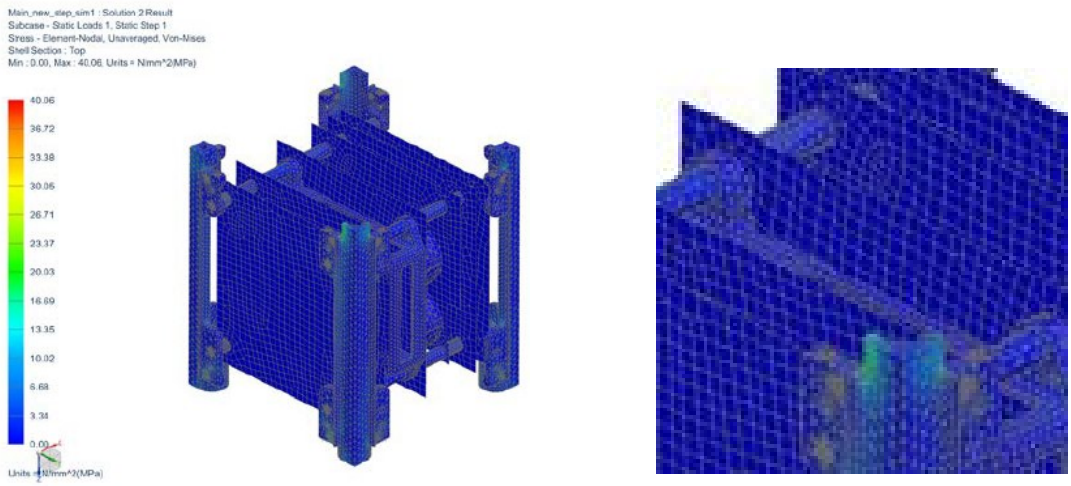

Figure 5.8 The area of maximum von Mises stress (MPa).

The value of maximum displacement deformation and the von Mises stress for Horizontal arrangement is illustrated in Table 5-5.

Table 5-5 The summarized displacements and maximum von Mises stress in a horizontal arrangement.

Case	Scenario	Longitudinal Axis (10.5g)	Transversal Axis (3.4g)	Maximum Displacement (mm)	Maximum von Mises stress (MPa)
1	X+	Y+	Z+	0.00405	41.22
2		Y-	Z+	0.0391	51.05
3		Y+	Z-	0.0410	65.22
4		Y-	Z+	0.0370	81.88
5	X-	Y+	Z+	0.0931	40.19
6		Y-	Z+	0.0487	38.24
7		Y+	Z-	0.0354	33.86
8		Y-	Z+	0.0289	33.56
9	Y+	X+	Z+	0.237	115.57
10		X-	Z+	0.262	108.52
11		X+	Z-	0.0311	32.89
12		X-	Z+	0.0319	43.61
13	Y-	X+	Z+	0.1031	63.61
14		X-	Z+	0.1163	42.14
15		X+	Z-	0.0480	54.83
16		X-	Z+	000589	49.23

The listed results in Table 5-5 indicate the maximum stress is 115.87 MPa, which is smaller than the yield strength (240 MPa) of AA6061 aluminum alloy. So, the structure is capable of withstanding the conditions it will experience during its launch when applying the extreme loading situation, as mentioned above.

Following the information provided in the ISILaunch condition documents, for the flight model, the payload's fundamental frequency must be above 20 Hz. The first 10 natural frequencies of UWE-4, are shown in Table 5-6, which are higher values than those specified in the launch vehicle qualification document [53].

Table 5-6 Natural frequencies.

Mode	Natural Frequency [Hz]	Mode	Natural Frequency [Hz]
1	286.9	6	556.3
2	336.1	7	701.8
3	442.3	8	799.3
4	449.3	9	805.6
5	488.5	10	820.6

5.2 The 1U CubeSat

Figure 5.9 shows a designed 1U CubeSat frame with the material Al-7075-T6 and 2mm thickness. This model is created using SolidWorks software [54].

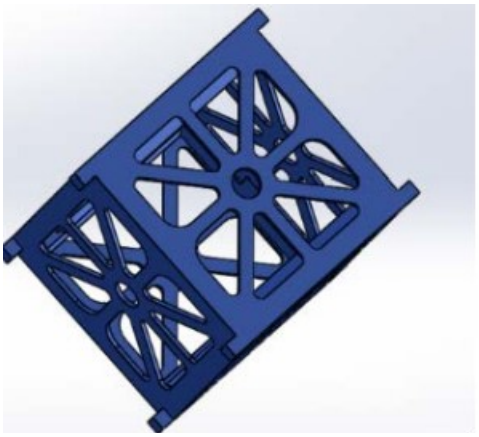

Figure 5.9 1U CubeSat frame [54].

The material properties of Al-7075-T6 is shown in Table 5-7.

Table 5-7 Material properties.

Material	Yield Strength (MPa)	Density (g/cm^3)	Poisson Ratio
Al-7075-T6	505	2.81	0.33

During launch the greatest stress occurs and the result of von Mises stress is shown in Figure 5.10.

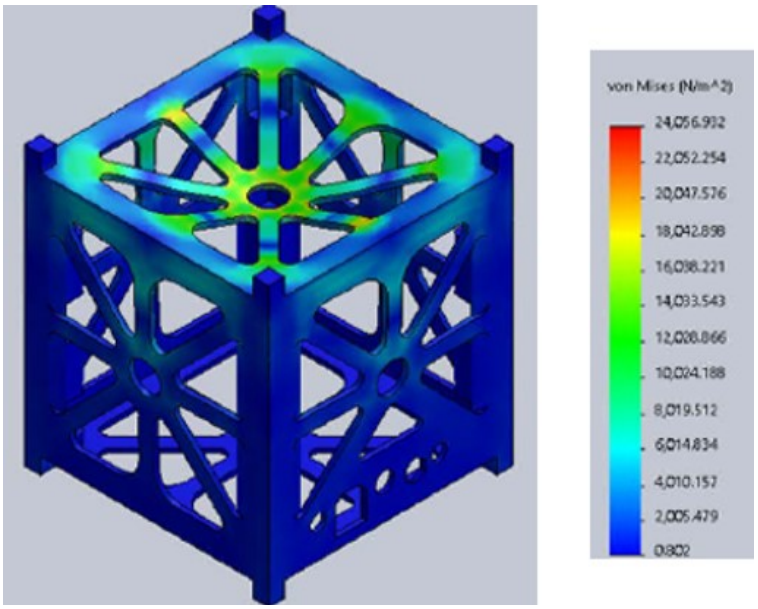

Figure 5.10 Stress analysis [54].

The value of maximum von Mises stress in this CubeSat is 240.56×10^{3}Pa and it is much smaller than the yield strength (505×10^{6} Pa). So, the survivability in this analysis shows a significant margin of safety like the analysis in chapter 3.

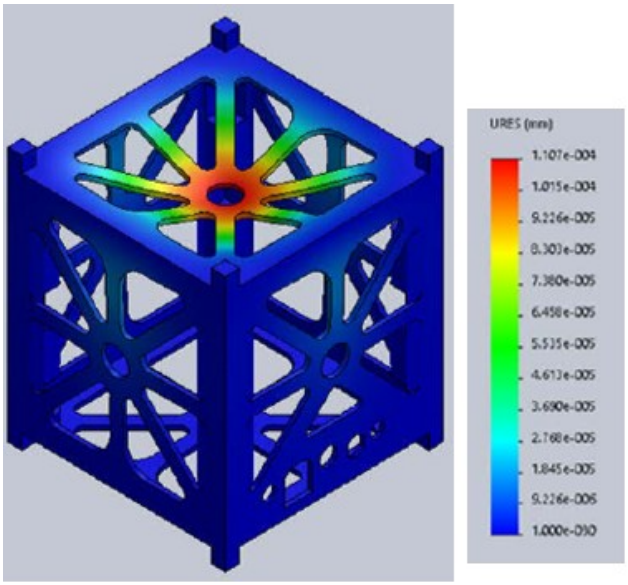

Figure 5.11 Displacement analysis [54].

The scale bowing structure in Figure 5.11 shows the maximum value of displacement (1.1×10^{-4} mm) on the top face during launch.

The value of maximum von Mises stress and maximum deformation in the above model is bigger than the values, mentioned in Chapter 3, in the designed CubeSat with AM method and AlSi10Mg material in this study. So, theoretically, the designed CubeSat in this study would be better.

5.3 The 3U CubeSat

For further validating the study in this thesis, showing the results for the case of a 3U CubeSat can also help with this claim. In this 3U CubeSat, Al 7075-T6 has been used due to having a higher yield strength (505 x 10^6 Pa). In this design 'Pumpkin CubeSat' model has been selected due to having some advantages, such as lowering the mass. In the static analysis, the lower legs of the four bases are fixed on the geometric center of the 3U CubeSat with the limit subjected to 50 g load. The von Mises stress results are illustrated in Figure 5.12 [55].

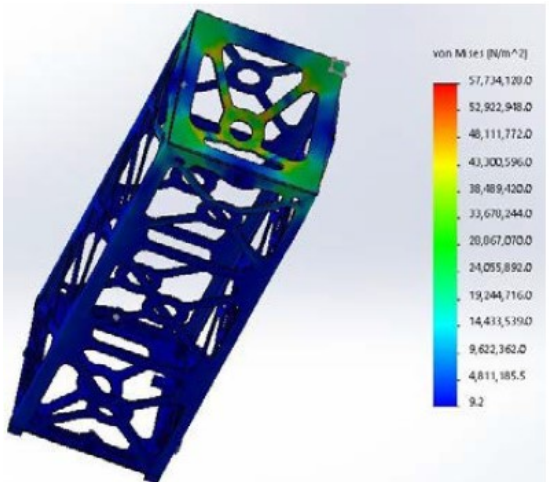

Figure 5.12 Von Mises stress results of 3U CubeSat (N/m²) [55].

The maximum von Mises stress under the worst-case scenario in this analysis is approximately 0.57 x 10^6 Pa (red colour), which is significantly lower than the yield strength (505 x 10^6 Pa) of aluminum alloy 7075-T6. In Figure 5.13, the deformation has happened in the center of the CubeSat, like the two previous CubeSats (i.e., 1U and UWE-4). The critical area in deformation values shows to occur in the center of CubeSat (Figure 5.13), although there is no threat due to having strong enough material.

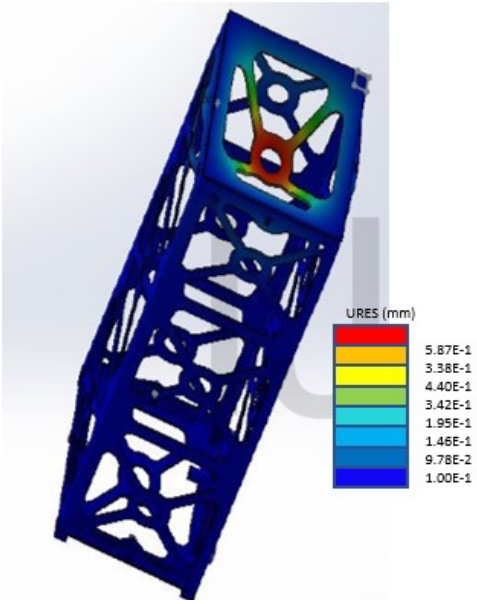

Figure 5.13 Displacement values on the CubeSat (mm) [55].

The FEA results of this study and the previous one in section 4-1 confirm that the designed CubeSat in the 3rd Chapter can withstand in the launch environment [38].

CHAPTER 6 CONCLUSIONS AND RECOMMENDATIONS FOR FUTURE WORK

6.1 Conclusions

While the overall final aim of this thesis was to use the AlSi10Mg and additive manufacturing method to fabricate a CubeSat, this has been restricted due to University closure arising from the COVID-19 pandemic. As a consequence, TO and FEA have been the focus required to simulate the model. During the course of this study, it was supposed necessary to manufacture a detailed database in regard to the additive manufacturing method(s) for the aluminum alloy(s). The following conclusions can be drawn, based on the theoretical investigation carried out in this thesis:

1- The possibility of manufacturing thin wall (2mm) AlSi10Mg alloys with LPBF is confirmed, due to having adequate process parameters, although the behaviour of aluminum depends on fabricating the aluminum with the parallel or perpendicular wall during LPBF.

2- It was also discovered that tetrahedral elements are preferred to be used for modelling the CubeSat's TO because of the satellite having a slightly complex geometry.

3- The results of the TO support the CubeSat's eliminated areas for the final design of the CubeSat. However, in terms of actual construction, the sharp edges, generated as a result of TO, must be converted to more rounded/smooth ones, due to having concentrated stress in the former state.

4- Currently, in the aerospace equipment, the additive manufacturing method has not really been used yet for satellite construction. In this study, the results obtained in

the NISA software by using FEA have confirmed the possibility of fabrication of the CubeSat, at least theoretically.

5- In terms of simulation of two CubeSats with 2 mm and 4 mm thickness: both of them could withstand in the defined environmental condition, although the weight-saving available with 2 mm promotes the suggested use of this dimension.

6- Although, it was observed that the stress concentration by enhancing the thickness will decrease. This decrease is attributed to the fact that by increasing the thickness of CubeSat its strength grows, and consequently, the mass of the CubeSat is increased.

6.2 Recommendations for Future Work

The study discussed through this thesis, relates to applying FEA aspects of TO and chassis design, with the ultimate aim of using the additive manufacturing method for building a CubeSat with the aluminum alloy AlSi10Mg. This has involved a review of a wide quantity of literature on 3D printing that affects the mechanical properties, which will have a potential implication on the fabricated CubeSat. As a next stage it is desirable to conduct a property evaluation of AlSi10Mg fabricated by LPBF additive manufacturing, and then actually build some preliminary CubeSat designs for mechanical property evaluation; this may be conducted at a reduced scale, for example, half-size models (1:2 scale ratio). The suggested approach should be abled to design the CubeSat and fabricate the model design(s) in suitable aluminum alloys by the additive manufacturing method and then doing the thermal and vibration tests on the CubeSat. The results must be validated by comparing the experimental and theoretical results, which are illustrated in Chapter 3. Rigorous approval of this method and the procedure can help to further promote the use of additive

manufacturing approaches for satellite applications. Subsequently, the design of more complicated models can be undertaken, with the ultimate aim of having more beneficial use of CubeSats in the aerospace industry.

BIBLIOGRAPHY

[1] "Canadian CubeSat Project - Canada.ca." Available: https://www.asc-csa.gc.ca/eng/satellites/cubesat/default.asp.

[2] A. Ampatzoglou and V. Kostopoulos, "Design, analysis, optimization, manufacturing, and testing of a 2U cubesat," Int. J. Aerosp. Eng., vol. 2018, 2018.

[3] ECSS, "Space engineering - Materials (ECSS-E-ST-32-08C Rev.1)," no. 1, pp. 1–81, 2014.

[4] D. Selva and D. Krejci, "A survey and assessment of the capabilities of Cubesats for Earth observation," Acta Astronaut., vol. 74, pp. 50–68, 2012.

[5] A. Toorian, "Cubesat design specification," CubeSat Program, Calif. Polytech. State, vol. 8651, no. 9, p. 22, 2009.

[6] N. Zosimovych and Z. Chen, "3D printing CubeSat: a low-cost mode of space exploration," Aeronaut. Aerosp. Open Access J., vol. 2, no. 5, pp. 320–324, 2018.

[7] C. Nieto-Peroy and M. R. Emami, "CubeSat mission: From design to operation," Appl. Sci., vol. 9, no. 15, pp. 1–24, 2019.

[8] A. Alanazi and J. Straub, "Engineering Methodology for Student-Driven CubeSats," Aerospace, vol. 6, no. 5, p. 54, 2019.

[9] T. Villela, C. A. Costa, A. M. Brandão, F. T. Bueno, and R. Leonardi, "Towards the thousandth CubeSat: A statistical overview," Int. J. Aerosp. Eng., vol. 2019, p. 13, 2019.

[10] "NASA Sets Coverage Schedule for CubeSat Launch Events , NASA." Available: https://www.nasa.gov/press-release/nasa-sets-coverage-schedule-for-cubesat-launch-events.

[11] D. Fluitt, "Feasibility Study Into the Use of 3D Printed Materials in Cubesat Flight Missions. [Master Thesis]. Department of Aerospace Engineering, California Polythechnic State University," 2012.

[12] "CubeSats: Tiny Payloads, Huge Benefits for Space Research , Space." Available: https://www.space.com/34324-cubesats.html.

[13] "Overview , Mars – NASA Solar System Exploration." Available: https://solarsystem.nasa.gov/planets/mars/overview/.

[14] J. Chin, "CubeSat 101: Basic Concepts and Processes for First-Time CubeSat Developers," 2017.

[15] S. Song, H. Kim, and Y. K. Chang, "Design and implementation of 3U CubeSat platform architecture," Int. J. Aerosp. Eng., vol. 2018.

[16] L. NanoRacks, "Current edition of Interface Document for NanoRacks Smallsat Customers," vol. 77058, no. 815, p. 14, 2013.

[17] “What’s inside a CubeSat? , Engineering360.” Available: https://insights.globalspec.com/article/12083/what-s-inside-a-cubesat.

[18] T. Prejean, “NanoRacks CubeSat Deployer (NRCSD) Interface Definition Document (IDD) NRCSD List of Revisions,” 2013.

[19] A. Israr, “Vibration and modal analysis of low earth orbit satellite,” Shock Viberation, 2014.

[20] S. J. Kang and H. U. Oh, “On-orbit thermal design and validation of 1 U standardized CubeSat of STEP cube lab,” Int. J. Aerosp. Eng., 2016.

[21] L. Rosen, D. Brent and B Gibson, “Additive Manufacturing Technologies.” Springer, (Dordrecht London), 2015.

[22] N. Guo and M. C. Leu, “Additive manufacturing: Technology, applications and research needs,” Front. Mech. Eng., vol. 8, no. 3, pp. 215–243, 2013.

[23] M. Nahmany, Y. Hadad, E. Aghion, A. Stern, and N. Frage, “Microstructural assessment and mechanical properties of electron beam welding of AlSi10Mg specimens fabricated by selective laser melting,” J. Mater. Process. Technol., vol. 270, pp. 228–240, 2019.

[24] C. Galy, E. Le Guen, E. Lacoste, and C. Arvieu, “Main defects observed in aluminum alloy parts produced by SLM: From causes to consequences,” Addit. Manuf., vol. 22, no. 2017, pp. 165–175, 2018.

[25] N. Read, W. Wang, K. Essa, and M. M. Attallah, “Selective laser melting of AlSi10Mg alloy: Process optimisation and mechanical properties development,” Mater. Des., vol. 65, pp. 417–424, 2015.

[26] R. Chou, A. Ghosh, S. C. Chou, M. Paliwal, and M. Brochu, “Microstructure and mechanical properties of Al10SiMg fabricated by pulsed laser powder bed fusion,” Mater. Sci. Eng. A, vol. 689, no. 2017, pp. 53–62, 2017.

[27] F. Calignano, G. Cattano, and D. Manfredi, “Manufacturing of thin wall structures in AlSi10Mg alloy by laser powder bed fusion through process parameters,” J. Mater. Process. Technol., vol. 255, no. 2018, pp. 773–783, 2018.

[28] K. Osakada and M. Shiomi, “Flexible manufacturing of metallic products by selective laser melting of powder,” Int. J. Mach. Tools Manuf., vol. 46, no. 11, pp. 1188–1193, 2006.

[29] “Metal Materials for 3D printing , EOS GmbH.” Available: https://www.eos.info/en/additive-manufacturing/3d-printing-metal/dmls-metal-materials.

[30] P. Ruano, L. L. Delgado, S. Picco, L. Villegas, and F. Tonelli, “We are IntechOpen , the world ’ s leading publisher of Open Access books Built by scientists , for scientists TOP 1 %,” Intech, p. 13, 2016.

[31] P. Gaudenzi, S. Atek, V. Cardini, M. Eugeni, and G. Graterol Nisi, “Revisiting the configuration of small satellites structures in the framework of 3D Additive Manufacturing,” Acta Astronaut., vol. 146, no. 2017, pp. 249–258, 2018.

[32] C. M. Wai, A. Rivai, and O. Bapokutty, “Modelling optimization involving different types of elements in finite element analysis,” IOP Conf. Ser. Mater. Sci. Eng., vol. 50, no. 1, 2013.

[33] C. B. Hilbert, “Tetrahedral mesh optimization and generation via topological transformations and gradient based node perturbation,” 2015.

[34] T. R. Chandrupatlla and A. D. Belegundu, “Introduction to finite elements in engineering 3rd Ed.” Prentice Hall, (New Jersey), 2002.

[35] S. E. Benzley, E. Perry, K. Merkley, B. Clark, and G. Sjaardema, “A Comparison of All-Hexahedral and All-Tetrahedral Finite Element Meshes for Elastic and Elasto-Plastic Analysis,” 4th Int. Meshing Roundtable, Sandia Natl. Lab., pp. 179–191, 1995.

[36] A. Ruggiero, R. D’Amato, and S. Affatato, “Comparison of meshing strategies in THR finite element modelling,” Materials (Basel)., vol. 12, no. 14, pp. 1–11, 2019.

[37] J. M. Gere and S. P. Timoshenko, “Mechanics of Materials.” KENT Publishing Company, (Boston: PWS), 1990.

[38] M. Cihan, A. Cetin, M. O. Kaya, and G. Inalhan, “Design and analysis of an innovative modular cubesat structure for ITU-pSAT II,” RAST 2011 - Proc. 5th Int. Conf. Recent Adv. Sp. Technol., pp. 494–499, 2011.

[39] R. Karunakaran, S. Ortgies, A. Tamayol, F. Bobaru, and M. P. Sealy, “Additive manufacturing of magnesium alloys,” Bioact. Mater., vol. 5, no. 1, pp. 44–54, 2020.

[40] “Magnesium Alloys - an overview , ScienceDirect Topics.” Available: https://www.sciencedirect.com/topics/materials-science/magnesium-alloys.

[41] M. Gieseke, C. Noelke, S. Kaierle, V. Wesling, and H. Haferkamp, “Selective laser melting of magnesium and magnesium alloys,” in Magnesium Technology 2013, Springer, 2013, pp. 65–68.

[42] N. T. Aboulkhair, M. Simonelli, L. Parry, I. Ashcroft, C. Tuck, and R. Hague, “3D printing of Aluminium alloys: Additive Manufacturing of Aluminium alloys using selective laser melting,” Prog. Mater. Sci., vol. 106, no. 2018, pp. 100–578, 2019.

[43] F. Trevisan, F. Calignano, M. Lorusso, and J. Pakkanen, “On the selective laser melting (SLM) of the AlSi10Mg alloy: Process, microstructure, and mechanical properties,” Materials (Basel)., vol. 10, no. 1, p. 76, 2017.

[44] N. T. Aboulkhair, M. Simonelli, L. Parry, I. Ashcroft, C. Tuck, and R. Hague, “3D printing of Aluminium alloys: Additive Manufacturing of Aluminium alloys using selective laser melting,” Prog. Mater. Sci., vol. 106, no. August 2018, p. 100578, 2019.

[45] T. D. Ngo, A. Kashani, G. Imbalzano, K. T. Q. Nguyen, and D. Hui, "Additive manufacturing (3D printing): A review of materials, methods, applications and challenges," Compos. Part B Eng., vol. 143, pp. 172–196, 2018.

[46] M. Leary, M. Mazur, J. Elambasseril, M. McMillan, and T. Chirent, "Selective laser melting (SLM) of AlSi12Mg lattice structures," Mater. Des., vol. 98, pp. 344–357, 2016.

[47] T. Strek, J. Michalski, and H. Jopek, "Computational Analysis of the Mechanical Impedance of the Sandwich Beam with Auxetic Metal Foam Core," Phys. Status Solidi Basic Res., vol. 256, no. 1, pp. 1–8, 2019.

[48] H. Steven and M. F. Huzain, "Requirements and design structure for Surya Satellite-1," IOP Conf. Ser. Earth Environ. Sci., vol. 149, no. 1, pp. 1–10, 2018.

[49] J. Fagerudd, "Stress simulation of the seam CubeSat structure during launch. [Master thesis]. Solid Mechanic, Engineering sciences Stockholm Sweden.," 2015.

[50] J. B. Ferguson, H. F. Lopez, K. Cho, and C. S. Kim, "Temperature effects on the tensile properties of precipitation-hardened Al-Mg-Cu-Si alloys," Metals (Basel)., vol. 6, no. 3, 2016.

[51] S. Chisabas, R. Stevenson, D. F. Cantor, L. G.eilson, and C. Lino, "Method for CubeSat Thermal-vacuum Cycling Test Specification.," 47th Int. Conf. Environ. Syst. 2017.

[52] J. Van Baren, "What is Random Vibration Testing?," Sound Vib., no. 9, pp. 9–12, 2012.

[53] A. Rathinam, "Design and Development of UWE-4 [Master of Applied Science Thesis]. Department of Space Science and Technology, Wurzburg University," 2015.

[54] K. Sekerere and T. Mushiri, "Finite element analysis of a cubesat," Proc. Int. Conf. Ind. Eng. Oper. Manag., vol. 2017, pp. 115–121, 2017.

[55] K. Alemayehu Adde and L. Rezene Elias, "Finite Element Analysis of 3U CubeSat Structure," Int. J. Sci. Eng. Res., vol. 9, no. 6, pp. 734–740, 2018.

APPENDIX A

RENDITION OF THE TO OF CUBESAT BY NISA

Introduction

NISA (Numerically Integrated elements for System Analysis) software is a proven software for Finite Element Analysis, used for solving the most complicated engineering problems. NISA can conduct various type of numerical analysis, such as analysis linear static, nonlinear direct transient, and heat transfer analysis. Both isoperimetric finite elements and conventional elements with higher order displacement function are available in NISA. Other elements like 3D composite solid, sandwich shell etc. are also available as well.

In NISA, the large number of material modals such as isotropic, orthotropic and laminated composite, elastoplastic material and also materials with temperature dependent properties. are available

NISA software suite also includes the pre- and post-processing modules (DISPLAY) program.

The NISA software's benefits are in developing high-quality industrial applications and having an optimized fabricated design, the results will be in the NISAOPT family of programs, SECOPT, STROPT and SHAPE. SECOPT optimizes a cross section beam. Optimization of structures of fixed shape is done by STROPT and SHAPE is for two- and three-dimensional continuum structural shape optimization.

Below are some of the capabilities which are offered by SHAPE:

- Shape optimization of large solid, shell, or planar structures for linear response under static loading, without boundary parametrization,
- As a separate selection, analysis of structural reaction,

- Shape optimization has two principal modes: limiting the shape variation with the current BCs, and allowing for creating new boundaries,
- There are not any restrictions on stress and strain constraints,
- Defining of fabrication constraints, followed by freezing special elements or nodes at the outset.

For conducting TO, NISA requires two types of files: NIS and OPT file. Below both of the files for the Cube presumably are explained.

NISA file

Design of the initial shape starts in the display shown below:

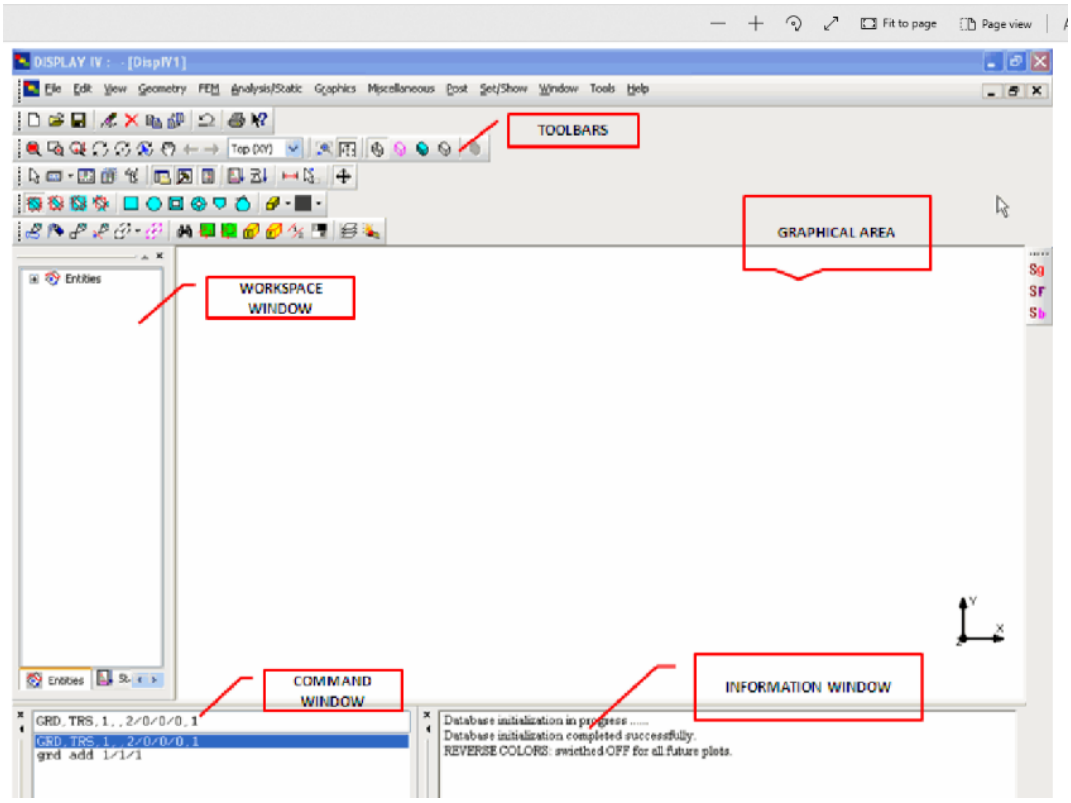

For creating the simple cube, the nodes of all corners of Cube are created in the following manner:

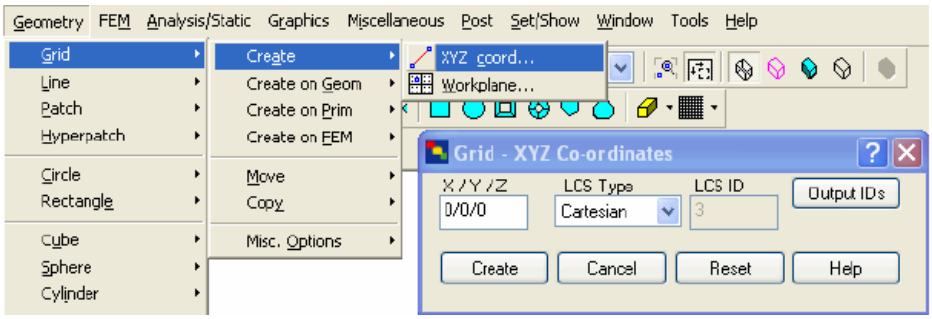

The below image shows the main points for creating the Cubic shape:

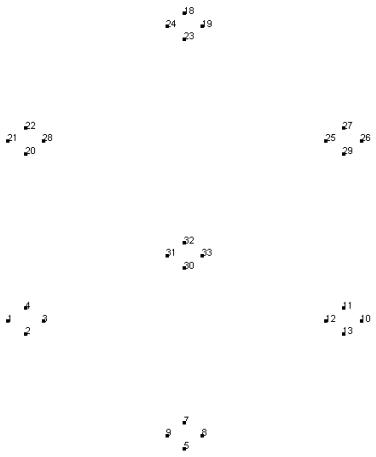

Then some patches are created as follows.

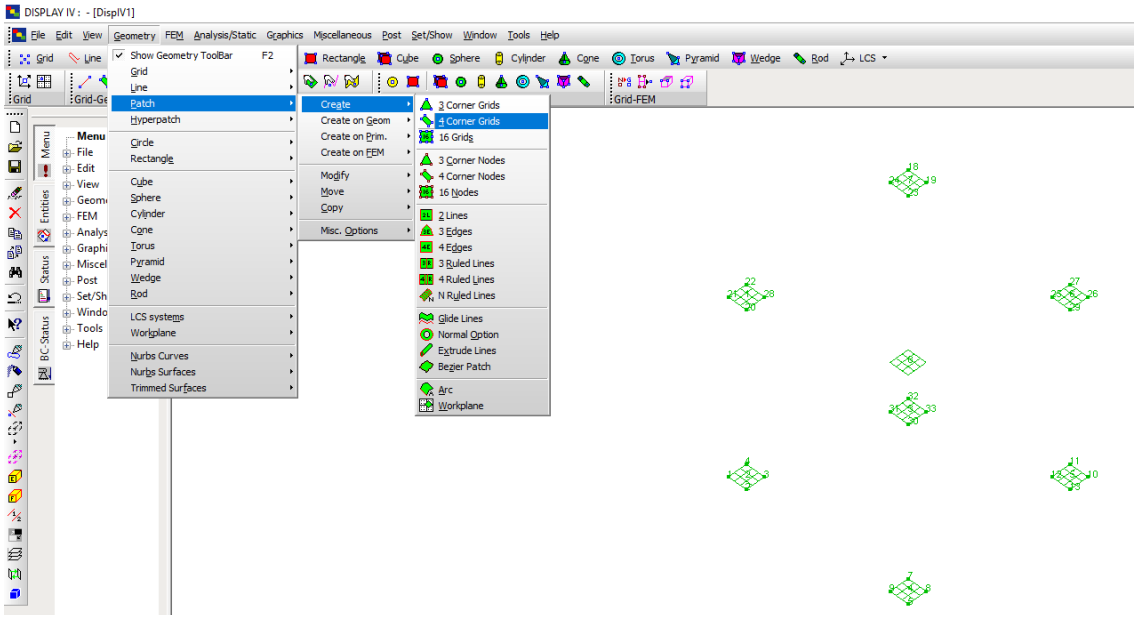

By using patches, hyper patches can be created following the direction below:

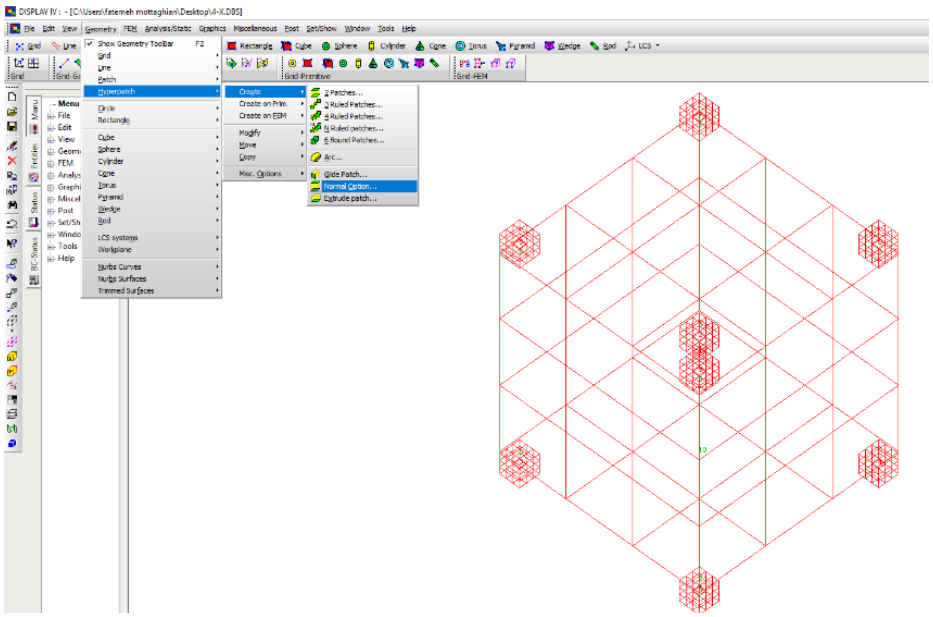

At this stage, the shape is ready to make elements by meshing. Meshing for TO is ideally hexahedral, following the approach below:

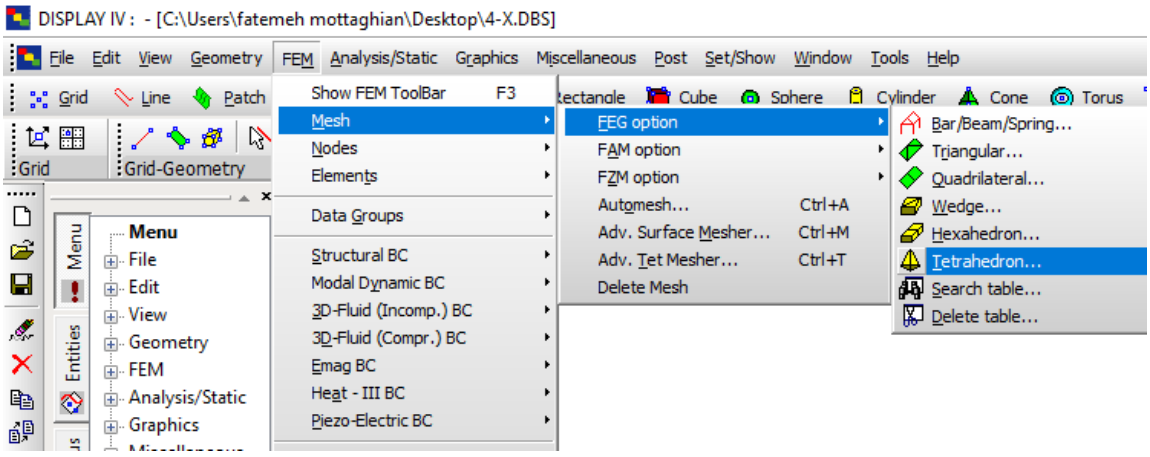

Finally, as an example, the shape shown below is created and then makes an empty CubeSat chassis, according to the thickness and size of the mesh, elements of the inside of the CubeSat can thus be eliminated. Then the material of the Cube should be defined:

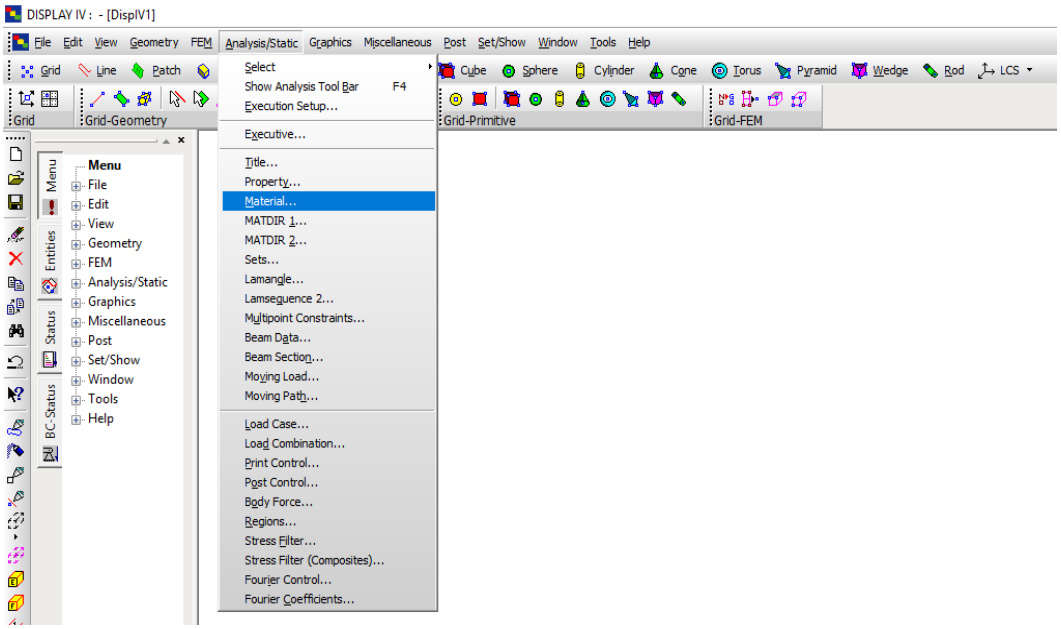

The information about the material such ad Modulus of elasticity and Poisson ratio can be inserted in the below icon:

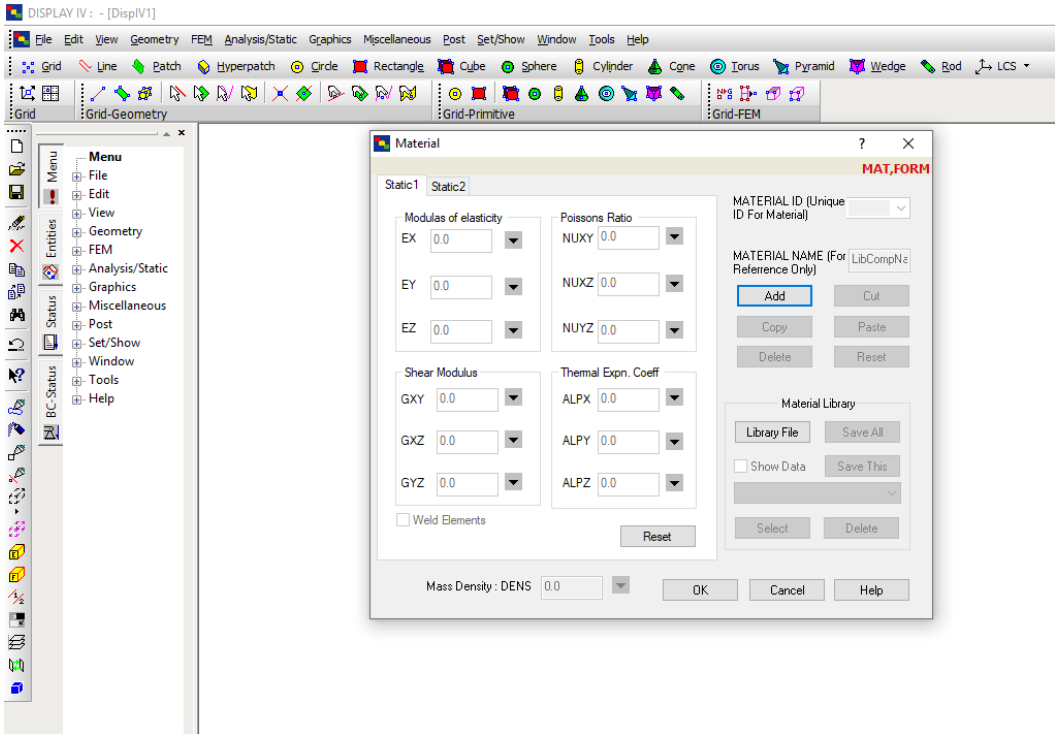

Then in the last part, the BC can be applied under the four conditions outlined. In the final shape below, the mesh (elements) and BC (yellow colour) are shown:

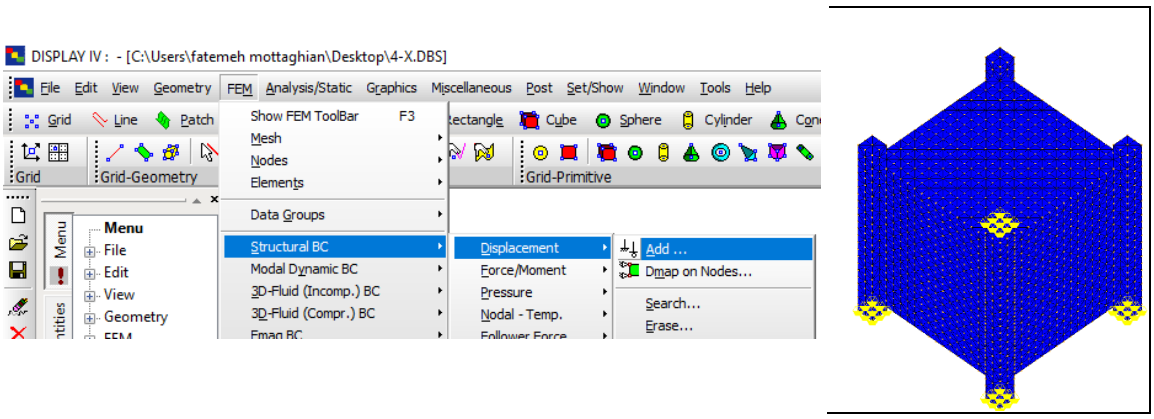

OPT file

In the optimization process, the information of OPT is entered in the OPT file. In this file at the very least, one stress must be specified, and in this specific file, the maximum von Mises file is entered. In this particular shape below, control commands are written in the OPT file. The format of inputting the data in the OPT file must be according to the NISA/OPT user's manual.

LIMIT = 300 (300 is the maximum number of iterations)

STEPS=10 (10 is the maximum number of design STEPS for this specific shape)

BREAK = OFF (OFF means the unnecessary ribs or bars in optimum design will be allowed to remain)

BOUND = ON (ON means the new internal boundaries can not be made)

CNSTRESS is the number of elements and it can be found from the .NIS file, and the number of elements in this file are 10880.

VMS is the value of maximum von Mise stress and in this specific study, it is 45e-4.

CNFABRICATIONAL ARE the frozen nodes and elements which should be defined in the OPT file to prevent them from making shape modification, for instance, in the CubeSat

all of the nodes and elements on the four columns are listed in the CNFABRICATIONAL option to avoid any changes.

ENDDATA should be defined to show the end of the file.

Run the files

After defining the OPT file for running or analyzing the file in OPT, the related information should be followed:

1- Select the analysis section,

2- Input the NIS file,

3- Click on the shape under the optimization category,

4- Enter the following type of file on the new page.

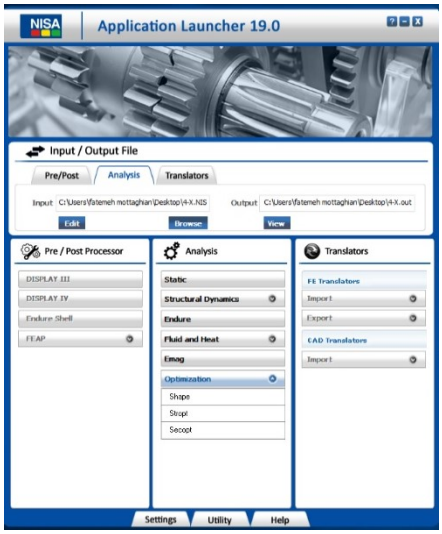

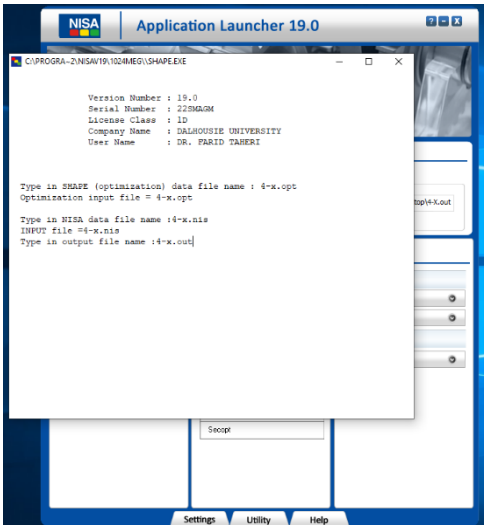

After acceptance, the analysis of the optimization will start and give some file results. The resulting files should be saved as a .NIS file and then opened. The file with the biggest number name would be the final optimized file. More information about TO in NISA can be found in the TO user manual.

MODELING THE CUBESAT (NISA)

For conducting FEA, NISA provides a more friendly user experience, and it is capable of analyzing the CubeSat design project efficiently and quickly. So, after evaluating different software packages, such as SolidWorks and Ls-Dyna, this software was selected in the present study After getting the results from TO, it would be possible to design a shape and remove the areas defined by TO in terms of an actual practical CubeSat manufacture.

Just as with TO explained in Appendix A, this part should start with defining specific nodes or grids. After the nodes, some patches and hyper patches should be defined to make the final shape. An example of the final shape is shown below:

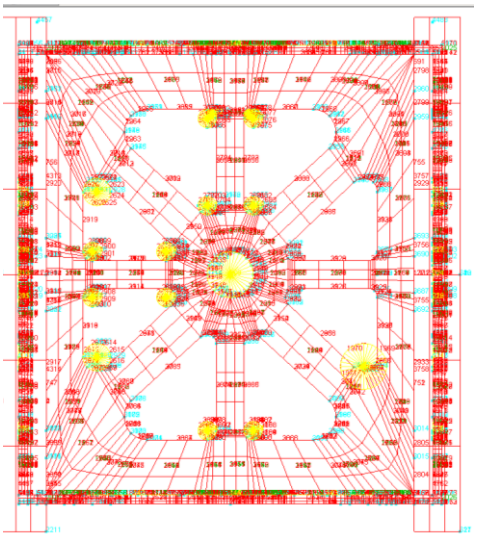

Then the hexahedron mesh has been defined for the model and the real BC must be applied (yellow color):

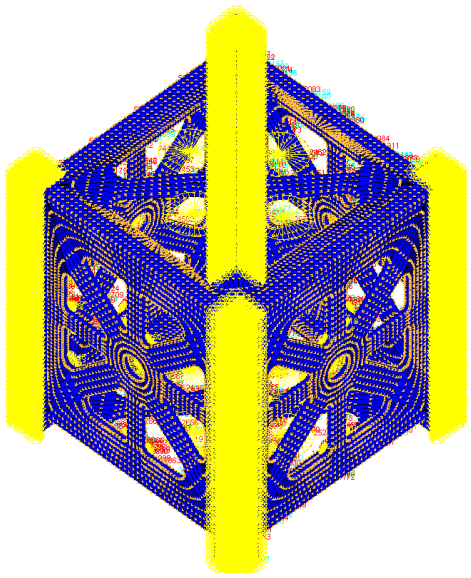

In the last part, the properties of the material should be entered, and then save the DBS file and subsequently save it as a NIS file. Finally, RUN the model and get the results in the file static26.

The explanation in Appendix A is not contained in all details. It only contains some critical options for this study. For getting more information about the rendition of TO and modelling any geometry, NISA has some user manuals for users.